#1

MASSACHUSETTS INSTITUTE OF TECHNOLOGY

RESEARCH LABORATORY OF ELECTRONICS

Technical Report 465 June 28, 1968

ANALYSIS OF DIGITAL AND ANALOG FORMANT SYNTHESIZERS

Bernard Gold and Lawrence R. Rabiner

(Manuscript received November 14, 1967)

Abstract

A digital formant is a resonant network based on the dynamics of second-order linear difference equations. A serial chain of digital formants can approximate the vocal tract during vowel production. The digital formant is defined and its properties are discussed, using z-transform notation. The results of detailed frequency response computations of both digital and conventional 'analog' formant synthesizers are then presented. These results indicate that the digital system without higher pole correction is a closer approximation than the analog system with higher pole correction. A set of measurements on the signal and noise properties of the digital system is described. Synthetic vowels generated for different signal-to-noise ratios help specify the required register lengths for the digital realization. A comparison between theory and experiment is presented.

TABLE OF CONTENTS

1. INTRODUCTION

The development of the theory of digital filters, [1, 2] which has taken place in recent years, has made it feasible to simulate a wide variety of speech communication devices on a general-purpose computer. The formant-type speech synthesizer is one of the devices that has been profitably simulated. [3-5] In this report digital filter theory is used to study the behavior of a serial formant synthesizer for generating vowel-like sounds. This type of synthesizer, which incorporates analog components, has been used in the OVE series [6] and in SPASS. [7] In the digital simulation of such devices, two new problems arise, sampling and quantizing. As is well known, a sampled-data filter is periodic in the frequency domain. Thus, a digital formant network obtained through simulation has a different frequency response from an analog formant network. As we shall see, the periodic frequency response of a digital formant network is actually a desirable feature, since it eliminates the need for the higher pole correction used with analog synthesizers. The quantization present in the finite-register-length computer creates two disturbances: inaccuracies in the formant positions, [8] and a wideband "noise" caused by round-off errors during the execution of the linear recursion. [9, 10] These effects place a lower limit on the length of the registers, and therefore must be seriously considered in simulating digital filters on computers with small register lengths. Also, the component advances in digital hardware raise the possibility that a special-purpose all-digital speech synthesizer or formant vocoder could become a feasible device; clearly, knowledge of register length constraints becomes major design information.

A widely held misconception is that difficulties arising in computer simulation of speech systems can be avoided by increasing the sampling rate; however, quantization problems will generally increase in severity as the sampling rate is raised. Thus a sound theoretical understanding of the effects of both sampling and quantizing are necessary for the design of digital speech synthesis programs or special-purpose digital hardware synthesizers.

In Section II the digital formant network will be defined and discussed, and we shall show that although linear analysis, with z-transform techniques, is applicable, it is necessary, in practice, to consider carefully the lengths of registers to be used in computation. In Section III we shall study the frequency response characteristics of digital formant synthesizers theoretically and experimentally, utilizing only the linear model. Our primary purpose is to find the extent to which a digital synthesizer can approximate the vocal-tract transfer function. In Section IV we shall derive the characteristics of the higher pole correction network used in analog synthesizers. In Section V the quantization problem will be reintroduced and theoretical and experimental methods will be applied to study the register-length problem.

II. DIGITAL FORMANTS

Using z-transform terminology, we can define the transfer function H(z) of a digital formant as

$$H(z) = \frac{(1-2r\cos bT+r^2)z^2}{z^2 - (2r\cos bT)z + r^2}, \tag{1}$$

where T is the sampling interval, and r and b are defined by reference to the z-plane pole-zero diagram of Fig. 1. The frequency response of the digital formant is obtained by setting $z = e^{j\omega t}$ in Eq. 1. Except for the frequency-dependent scale factor in the numerator, this frequency response can be obtained geometrically from Fig. 1 by measuring the distance from any point on the unit circle (at an angle ωT) to the poles, the magnitude of $H(e^{j\omega T})$ being inversely proportional to the product of the distances from that point to the poles, and directly proportional to the product of the distances to the zeros, which in our case are unity. The significance of r is illuminated by letting $r = e^{-aT}$, so that the parameter a may be interpreted as a half-bandwidth radian frequency. It can be seen from Eq. 1 that H(1) = 1, which shows that the digital formant has the correct DC gain independent of the resonant frequency; this is accomplished by making the numerator dependent on the pole positions so as to always satisfy this condition on the DC gain.

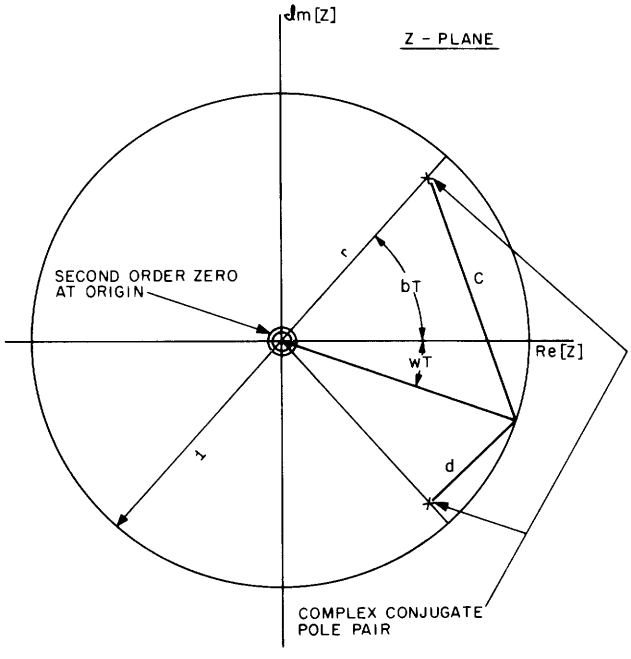

Fig. 1. Z-plane pole-zero diagram for digital formant.

The transfer function H(z) can be realized approximately in a variety of ways; approximately because no indication of the quantization problem appears in Eq. 1. Thus, the recursive relation,

$$y(nT) = 2r\cos(bT)\,y(nT-T) - r^2 y(nT-2T) + (1-2r\cos bT+r^2)\,x(nT) \tag{2}$$

permits the variables x(nT) and y(nT) to take on any real values, whereas in the computer these variables are always contained in finite-length registers. A convenient way of representing the computation of Eq. 2 is by the "network" of Fig. 2. The triangular boxes represent unit delays of time T, the rectangular boxes are the fixed multipliers,

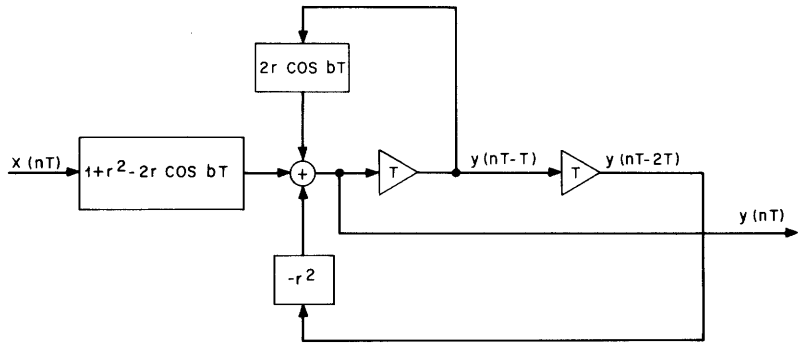

Fig. 2. Digital network representation #1 of a single formant.

that is, the coefficients of the recursive equation (2), and the sum is represented by the circle with the plus sign. These elements are the basic ones for any general system of linear recursions. Computationally, Fig. 2, as well as Eq. 1, is interpreted as follows: a new sample x(nT) appears at the input. This signal is multiplied by the fixed number $(1+r^2-2r\cos bT)$; the multiplications indicated by the other two rectangular boxes are carried out, all indicated products are summed, and the appropriate register transfers are performed, to fulfill Eq. 2. The system is now ready for a new input sample.

Because of the linearity of the network of Eq. 1, it is possible to exchange the sequence of operations. For example, Fig. 3 represents a different sequence of computations leading to the same transfer function H(z) in Eq. 1. Although the difference

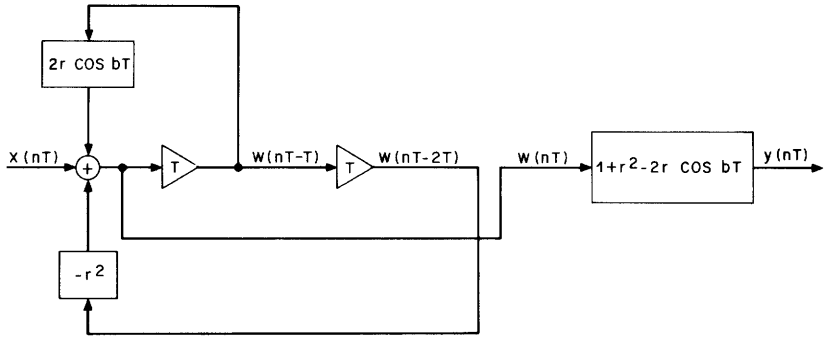

Fig. 3. Digital network representation #2 of a single formant.

between the networks of Figs. 2 and 3 may seem trivial, if one remembers that the actual computations involve finite register lengths, these differences may be significant. To illustrate, assume that $1 + r^2 - 2r \cos bT = .01$ for a given system. If an input sample x(nT) of magnitude 20 appeared, the product is less than unity and would be truncated to zero. Thus, the system of Fig. 2 exhibits a noticeable nonlinear effect if the input signal level is too small. The same signal applied through the network of Fig. 3, however, might not exhibit such an effect because the first portion of the network (up to the

final multiplier) could have boosted the signal level to well above 100. Thus, although the "linear" behavior of the networks of Figs. 2 and 3 is identical, the actual behavior of the two could be markedly different.

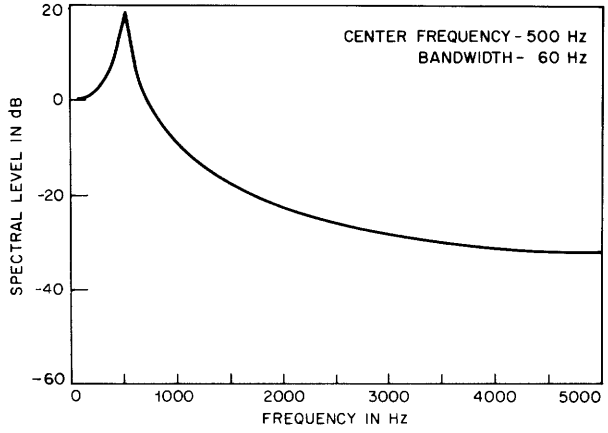

Fig. 4. Frequency response of a digital formant.

In the remainder of this section and until Section V, the finite-register-length problem will be ignored and the frequency response characteristic of the digital formant network will be studied, with Eq. 1 and Fig. 1 used as the starting point. H(z) actually has an infinity of poles, occurring at the frequencies $(\pm b/2\pi \pm nf_r)$Hz with n = 0, 1, 2, ... and $f_r = 1/T$. Thus, the frequency response of the digital formant is periodic, with a period equal to the sampling rate f_r. This well-known property of sampled system is made explicit for the digital formant by writing $|H(e^{j\omega T})|$, that is, the magnitude of H(z) at any angle ωT on the unit circle,

$$|H(e^{j\omega T})| = \frac{1 - 2r\cos bT + r^2}{[1+r^2-2r\cos(\omega-b)T]^{1/2}\,[1+r^2-2r\cos(\omega+b)T]^{1/2}}. \tag{3}$$

$|H(e^{j\omega T})|$ is clearly periodic in the angle ωT with period 2π, and this is equivalent to periodicity in frequency with period f_r. Also, the resonance effect is clearly seen by means of the left side of the denominator, which becomes small when $(\omega-b)T = n\pi$, n = 0, ±1, ±2, ..., thereby yielding the type of result sketched in Fig. 4.

III. DIGITAL FORMANT SYNTHESIZER

It is, of course, the repetitive nature of the frequency response of the digital formant network which suggests that it resembles more closely (than does the analog formant network) the repetitive frequency response of the vocal tract. The upper curve of Fig. 5 indicates the frequency response of an acoustic tube excited at one end and open at the other. (We have assumed equal bandwidths for all resonances.) This simple model is a representation of an ideal neutral vowel. If the sampling time T is chosen to be 0.5 msec, then a digital formant at 500 Hz has repetitive modes at the same frequencies as the tube, while a single analog formant at 500 Hz does not at all resemble the tube. The rest of the curves in Fig. 5 show a comparison among 5 formant, analog, and digital ($T = 10^{-4}$ sec) approximations to the tube. It is clear that, for this case, the digital system is a good approximation to the tube, whereas the analog system needs a correction network to compensate for the high-frequency fall-off characteristics of cascaded analog formants.

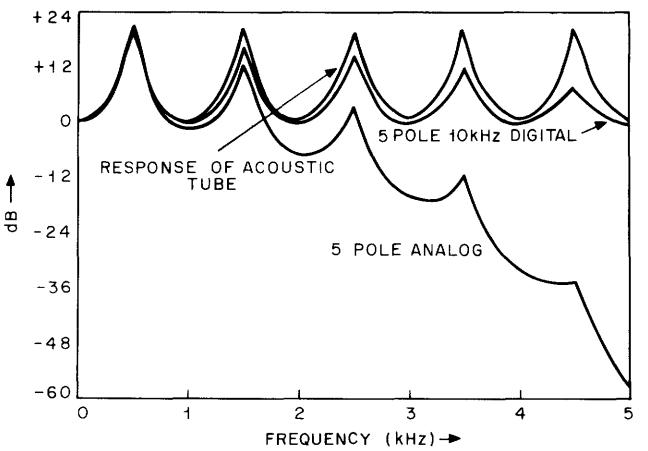

Fig. 5. Digital and analog approximations to the transfer function of an acoustic tube, open at one end and closed at the other.

A mathematical representation of the distributed parameter vocal-tract system is quite difficult, and we are not able (nor have we really tried) to create a purely theoretical argument for choosing either the digital or analog formant as the better approximation to the actual vocal tract. It can be argued, however, that an analog formant synthesizer consisting of a large number of resonators and higher pole correction can serve as a criterion for the correct frequency response characteristic of the vocal tract. The standard that we have adopted uses 10 cascade resonators and an improved higher pole correction. (The nature of this improvement will be examined in Section IV.) We denote this standard configuration #1. In the rest of this section we shall present and discuss experimental comparisons between system #1 and the three following systems.

#2 10-pole digital formant synthesizer with 20-kHz sampling.

#3 5-pole digital formant synthesizer with 10-kHz sampling.

#4 5-pole analog formant synthesizer with improved higher pole correction.

As we have indicated, we have guessed that a digital synthesizer does not need any higher pole correction, and no such network is used in systems #2 and #3.

Figure 6 represents system #3. The resonance frequencies F_1, F_2, and F_3 are variable and correspond to the three lowest resonances in the voiced-speech spectrum,

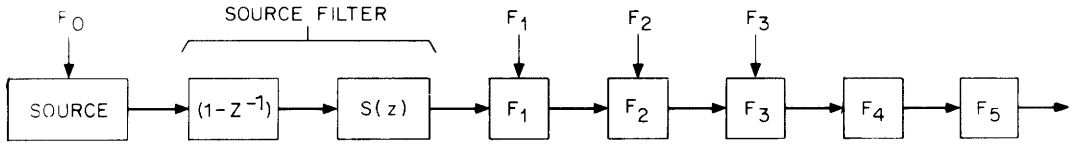

Fig. 6. 5-pole, 10-kHz digital formant synthesizer.

and thus determine, for example, the particular vowel sound that is generated. The fixed resonators F_5 and F_4, with resonances at 4500 and 3500 Hz, help provide the correct over-all spectrum shape. S(z) represents a formantlike digital network, which has been recommended as a suitable source filter, and the transfer function $1 - z^{-1}$ approximates the mouth-to-transducer radiation. Each of the digital formant networks is of the form given in Figs. 2 or 3 and has a transfer function of the form of Eq. 1. Thus the transfer function of the entire synthesizer is given by

$$F(z) = S(z)(1-z^{-1}) \prod_{i=1}^{5} F_i(z), \tag{4}$$

with

$$F_i(z) = \frac{\left(1+r_i^2-2r_i \cos b_i T\right) z^2}{z^2 - (2r_i \cos b_i T)z + r_i^2}.$$

For the 10-pole digital, 20-kHz system #2, five additional digital formants at 5500, 6500, 7500, 8500 and 9500 Hz have been inserted into the chain of Fig. 6.

Each digital formant is specified by values of the parameters r_i and b_i. To change these parameters into frequencies, we use the relations $r_i = e^{-2\pi g_i T}$ and $b_i = 2\pi f_i$, so that f_i is the resonance frequency, and g_i is the half-bandwidth expressed as a Herzian frequency. Table 1 shows the values of f_1, f_2, and f_3 chosen[11] for each of the 10 vowel sounds analyzed by us. Table 2 shows the bandwidths of all of the formants; the same fixed values were used throughout for both digital and analog cases. The values and extrapolations for higher formants are based on data by Dunn.[12]

Table 1. Formant frequencies for the vowels.

TYPEWRITTEN SYMBOL FOR VOWEL	IPA SYMBOL	TYPICAL WORD	F_1	F_2	F_3
IY	i	(beet)	270	2290	3010
I	I	(bit)	390	1990	2550
E	ɛ	(bet)	530	1840	2480
AE	æ	(bat)	660	1720	2410
UH	ʌ	(but)	520	1190	2390
A	a	(hot)	730	1090	2440
OW	ɔ	(bought)	570	840	2410
U	U	(foot)	440	1020	2240
OO	μ	(boot)	300	870	2240
ER	3	(bird)	490	1350	1690

Table 2. Analog and digital resonator bandwidths and center frequencies.

RESONATOR	CF (Hz)	BW (Hz)	Q
F1	Variable	60	Variable
F2	Variable	100	Variable
F3	Variable	120	Variable
F4	3500	175	20
F5	4500	281	16
F6	5500	458	12
F7	6500	722	9
F8	7500	1250	6
F9	8500	2125	4
F10	9500	4750	2

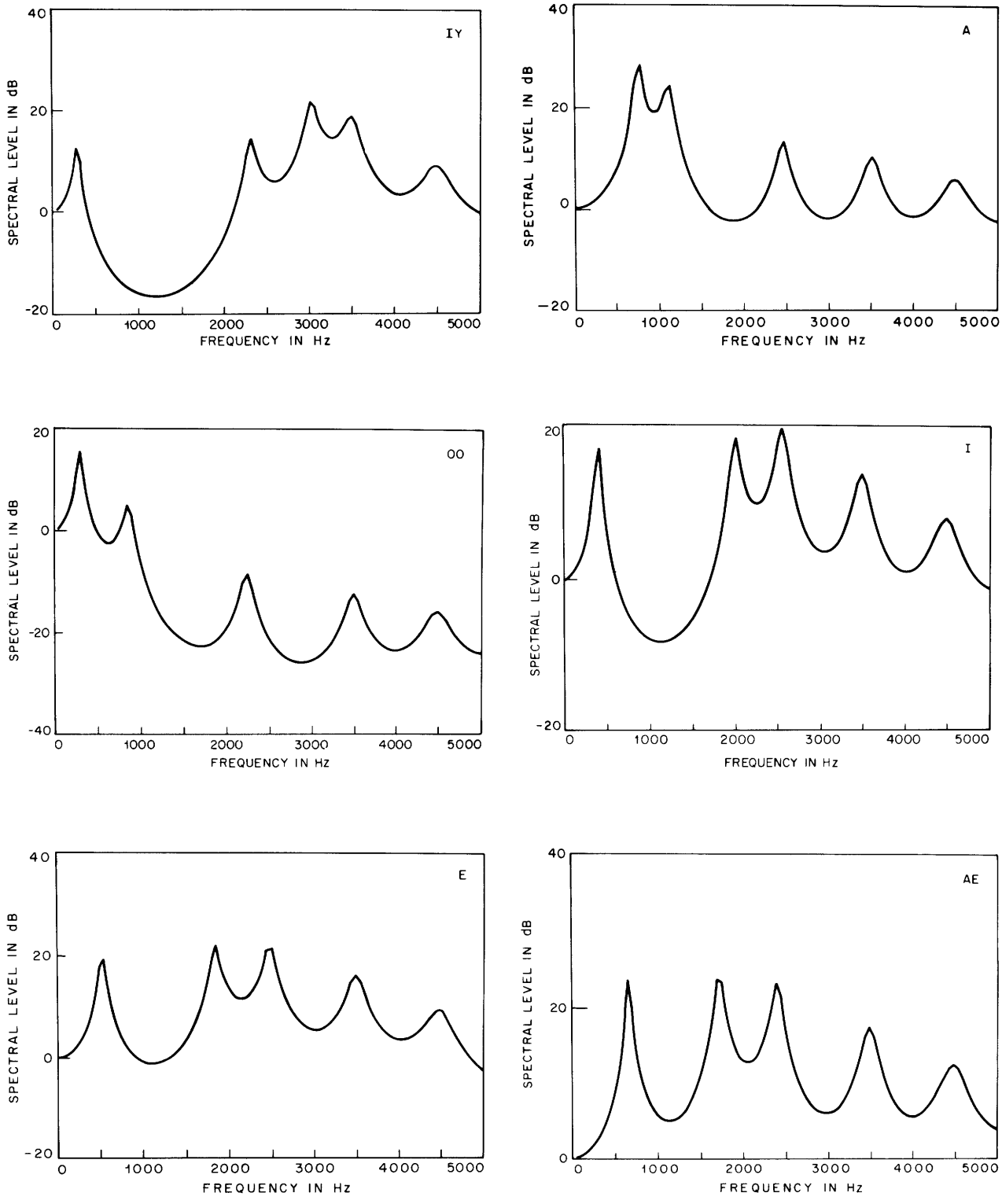

Fig. 7. Case #1. Amplitude frequency response — 10-pole analog.

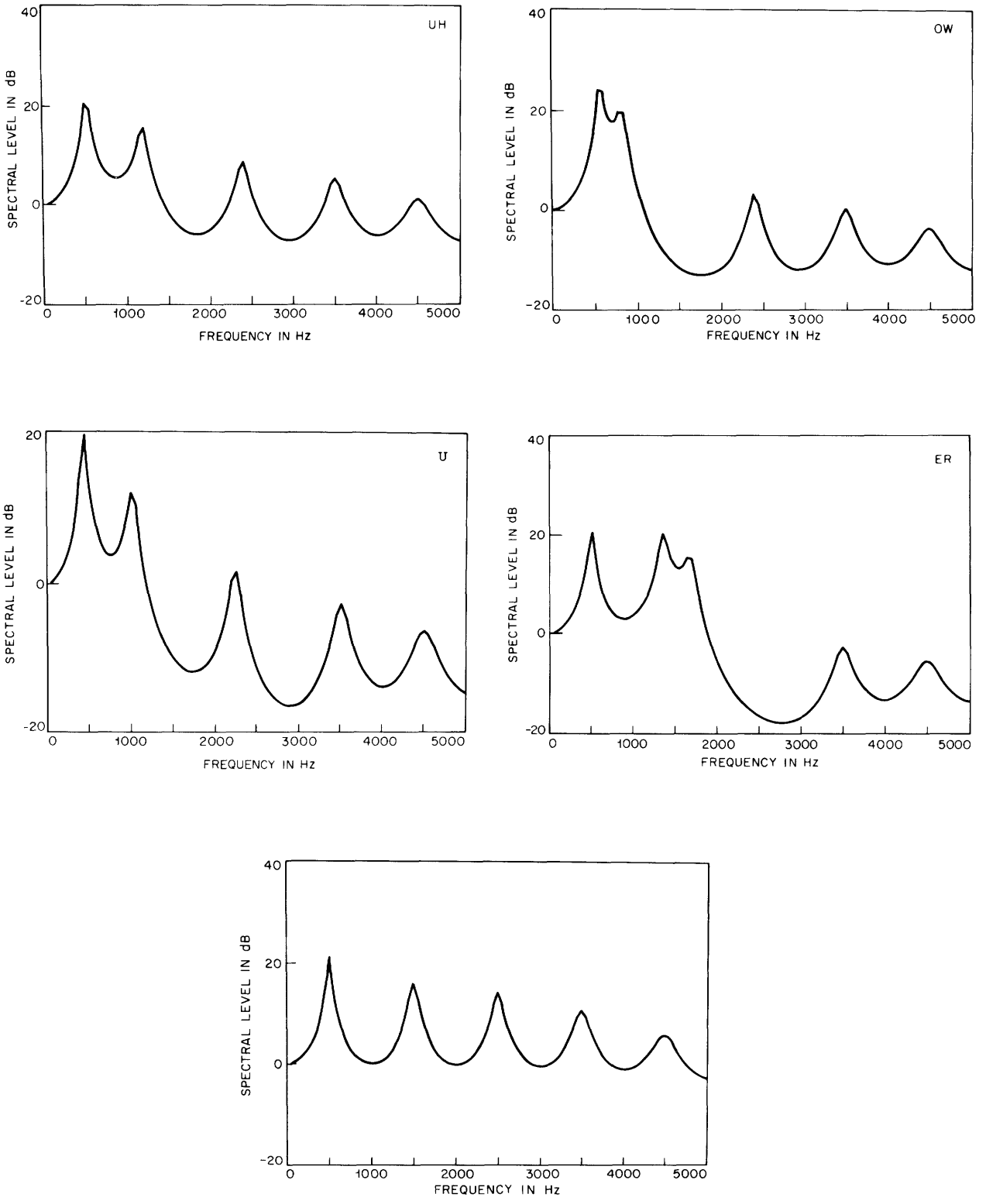

Fig. 7. Case #1. 10-pole analog (concluded).

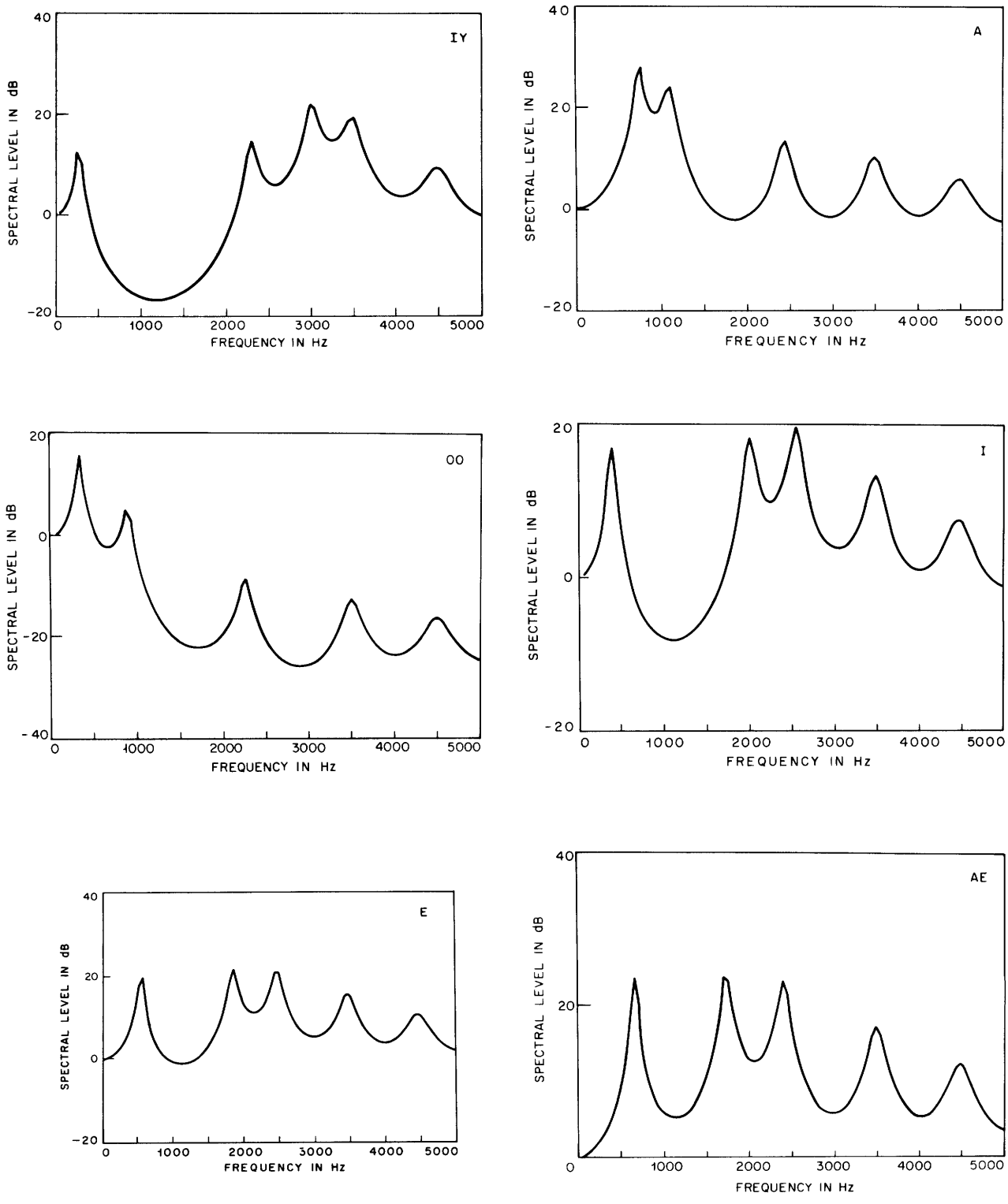

Fig. 8. Case #2. Amplitude frequency response – 10-pole digital, 20-kHz sampling frequency.

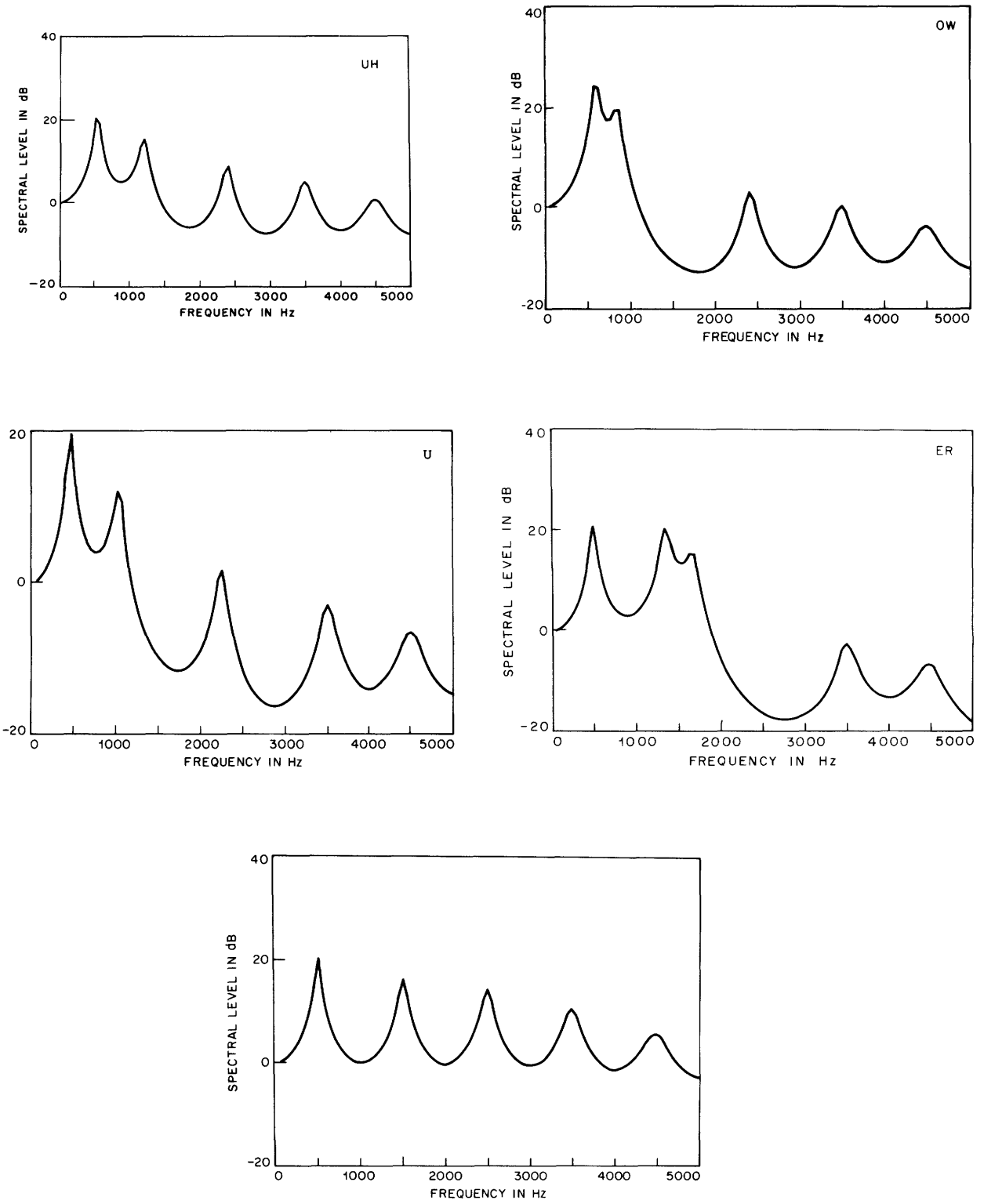

Fig. 8. Case #2. 10-pole digital, 20-kHz sampling frequency (concluded).

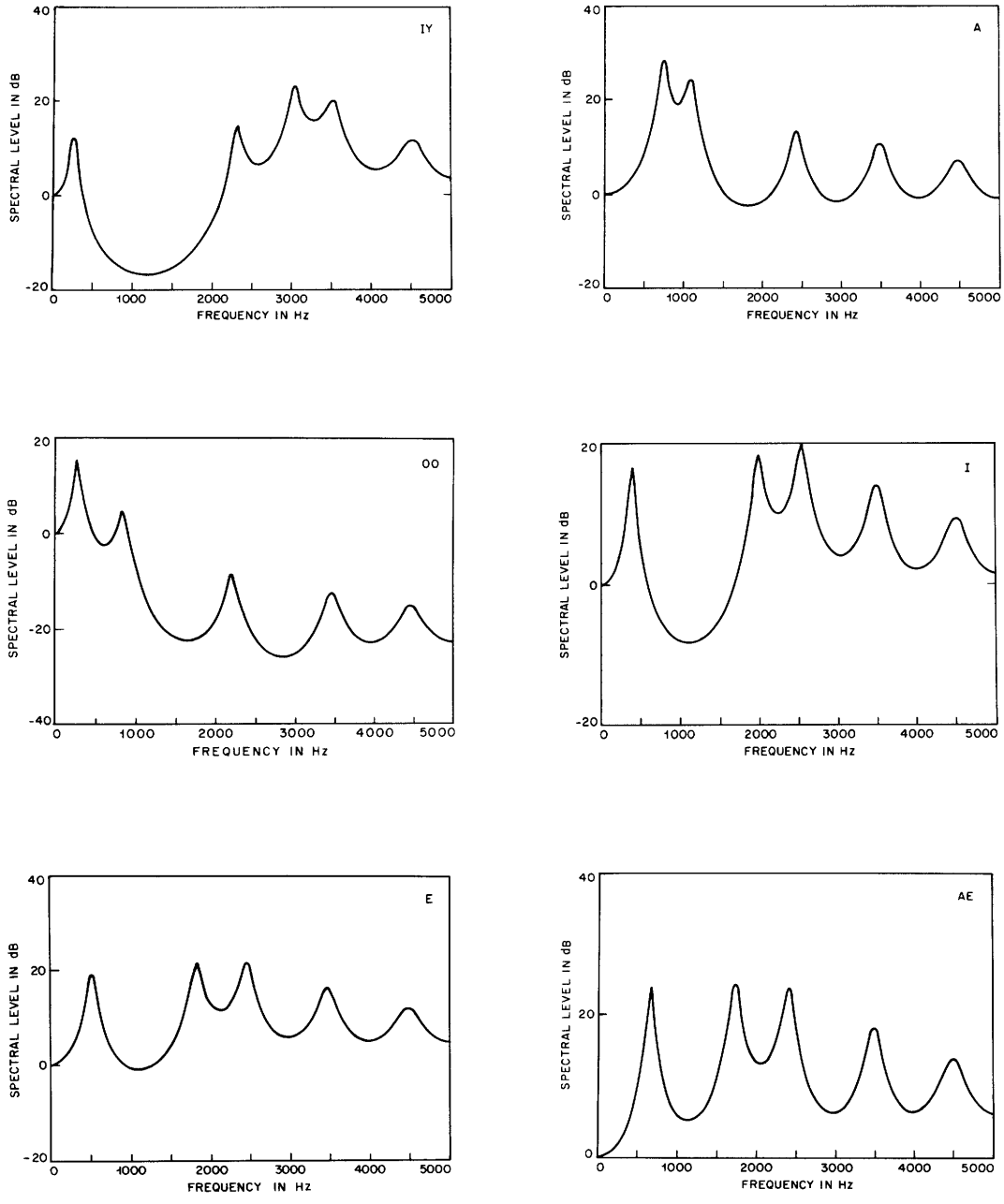

Fig. 9. Case #3. Amplitude frequency response – 5-pole digital, 10-kHz sampling frequency.

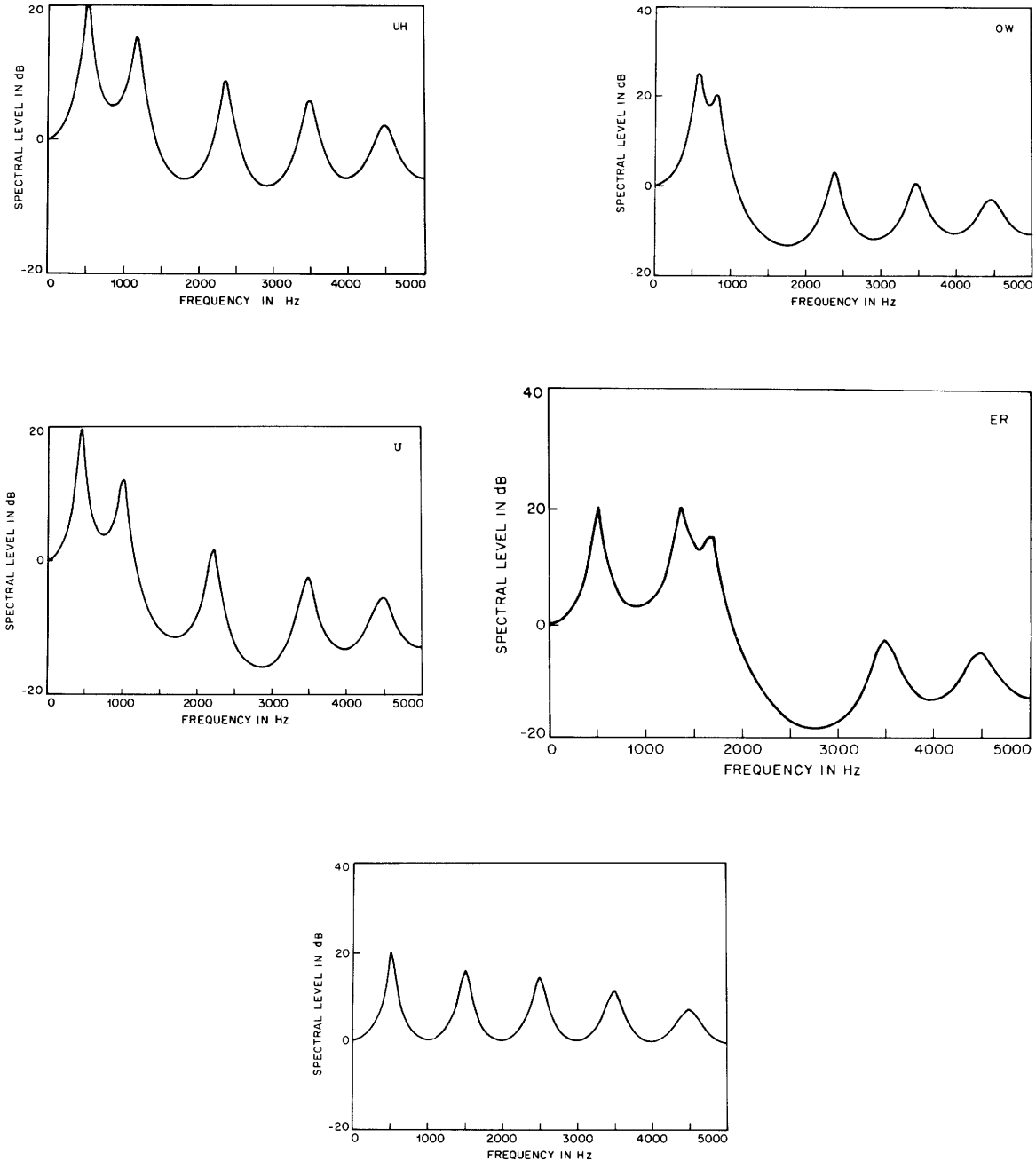

Fig. 9. Case #3. 5-pole digital, 10-kHz sampling frequency (concluded).

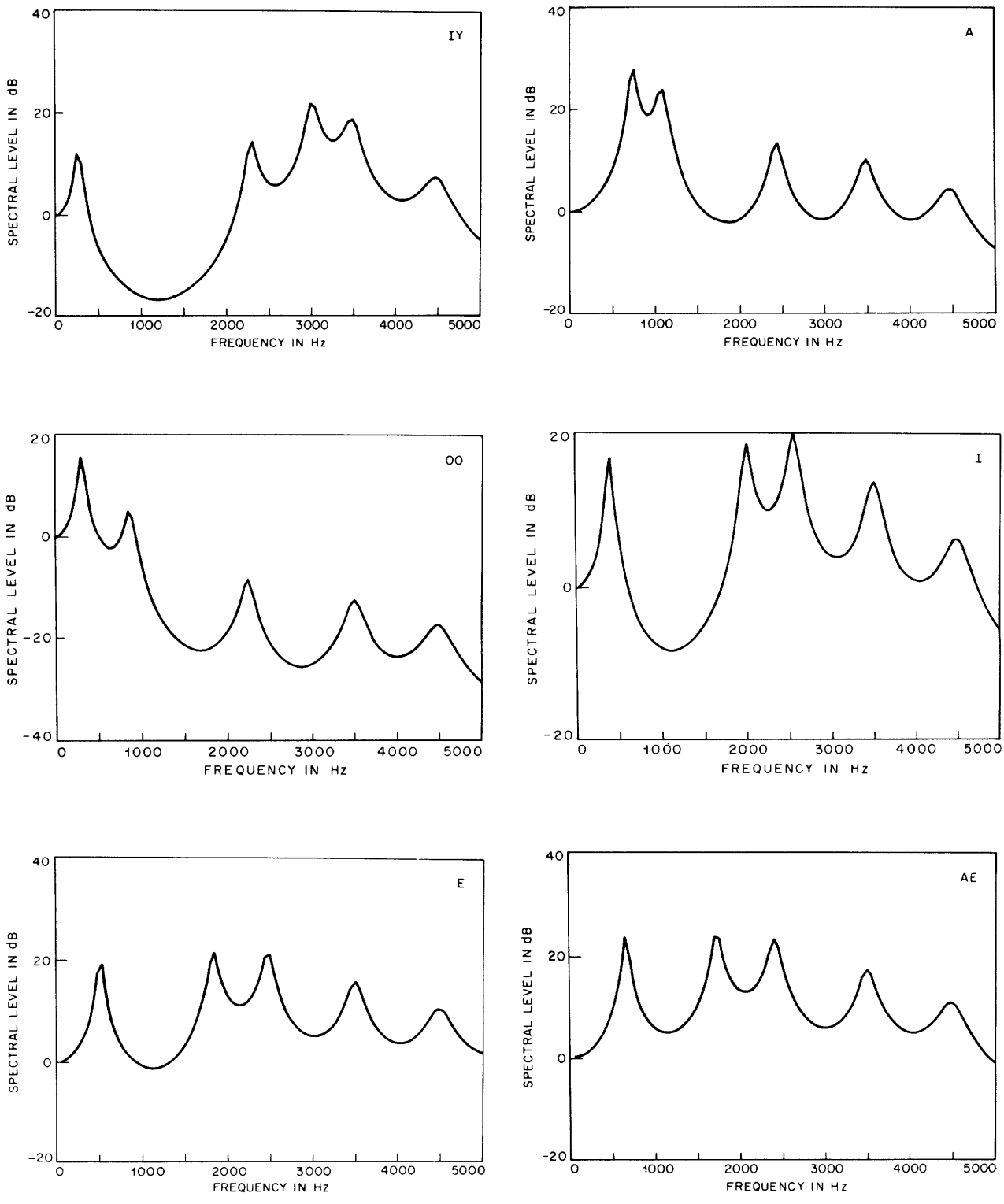

Fig. 10. Case #4. Amplitude frequency response – 5-pole analog.

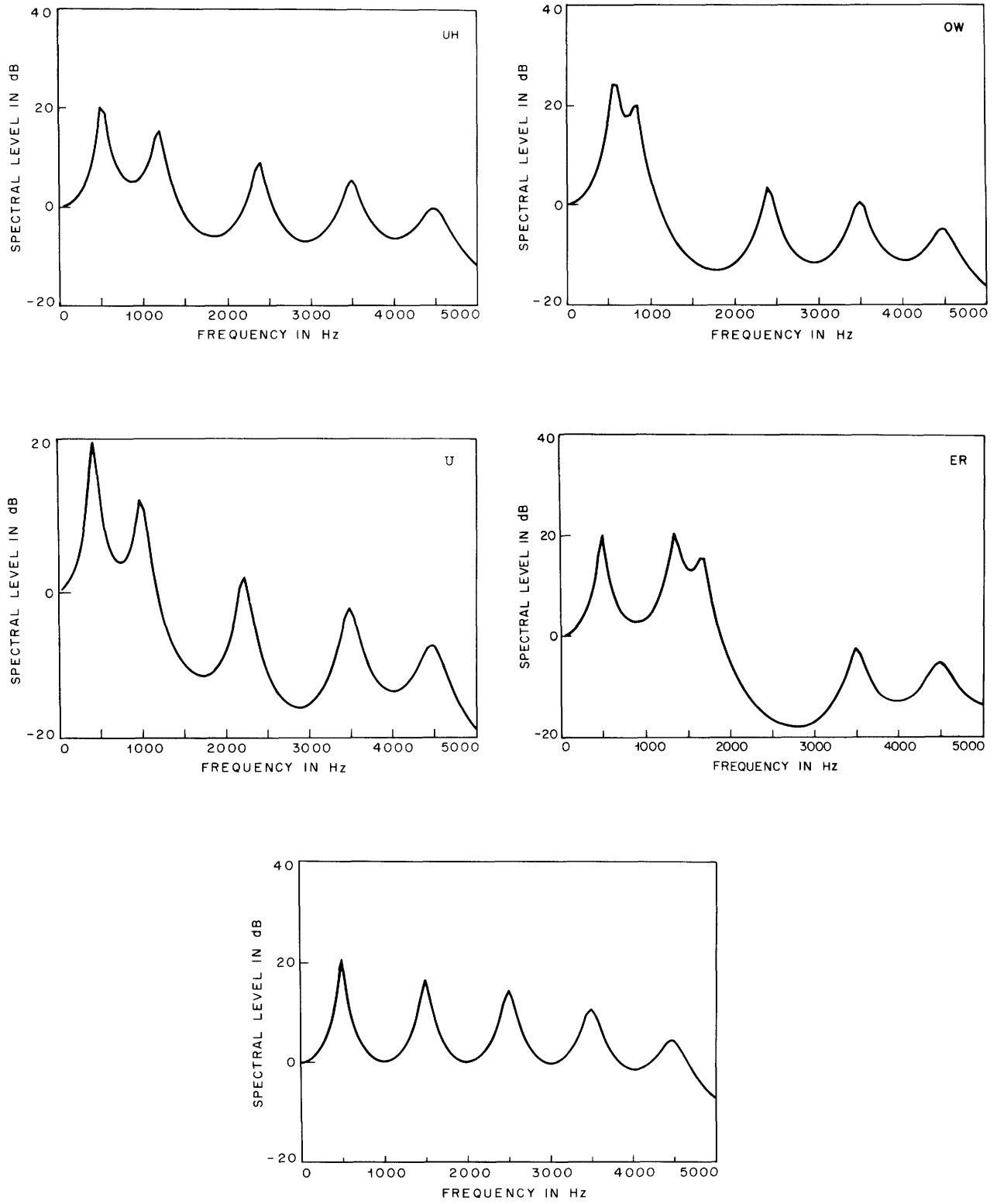

Fig. 10. Case #4. 5-pole analog (concluded).

The analog formant synthesizers are the classical vowel synthesizer treated by Gunnar Fant.[13] They consist of 5 (for case #4) or ten (for case #1) analog resonators of the form

$$H(s) = \frac{s_1 s_1^*}{(s-s_1)(s-s_1^*)}, \tag{5}$$

an additional analog resonator of 200-Hz center frequency and 250 Hz bandwidth for the source filter, a differentiator, and a higher pole correction (which will be described in greater detail in Section IV).

Given the 10 vowels listed in Table 1, a total of 40 frequency response curves had to be experimentally determined in order to compare systems #1, #2, #3 and #4. The measurements for systems #2 and #3 were made by passing a unit sine wave through a simulation of the system and determining the peak output amplitude after the transient response of the system had subsided. The frequency of the input was varied from 50 Hz to 5000 Hz in 50-Hz steps. The data for systems #1 and #4 were theoretically calculated from the synthesizer system functions. Figures 7 through 10 show results for the four systems for each of three vowels. In these figures, the logarithmic magnitude (in dB) is plotted on a linear frequency scale. The contribution of the source filters is omitted from these curves and will be treated separately. No generality is lost thereby, since, as we shall see, it is a simple matter to combine the effects of the source and resonators.

Figures 11, 12 and 13 show plots of the differences between spectral magnitudes of systems #2, #3, and #4 relative to the reference system #1 for each of the vowels IY, A, and OO. (Table 1 shows the IPA symbols and our typewritten equivalents for the vowels.) We see that the 10-pole, 20-kHz digital system #2 is extremely close to the reference system. This strongly indicates that higher poles of the vocal-tract transfer function are automatically, and more or less correctly, taken into account by the repetitive nature of the digital formant frequency response. We also note that this intrinsic correction is actually more accurate than the quite good analog higher pole correction used in our computations. These results are generally valid for all of the vowels.

Comparison of system #3 with the standard is of particular interest, since a 5-pole, 10-kHz system appears to be a good compromise design for a possible hardware version of a digital formant synthesizer. The peak difference between the magnitude curves for systems #1 and #3 is listed in Table 3, for each vowel. On the basis of this result, it seems reasonable to expect that a 5-pole, 10-kHz digital vowel synthesizer should produce synthetic vowels of quality comparable to a well-designed 5-pole analog vowel synthesizer that includes a higher pole correction. Informal listening re-enforces this expectation.

Inclusion of the source filters for both analog and digital cases slightly

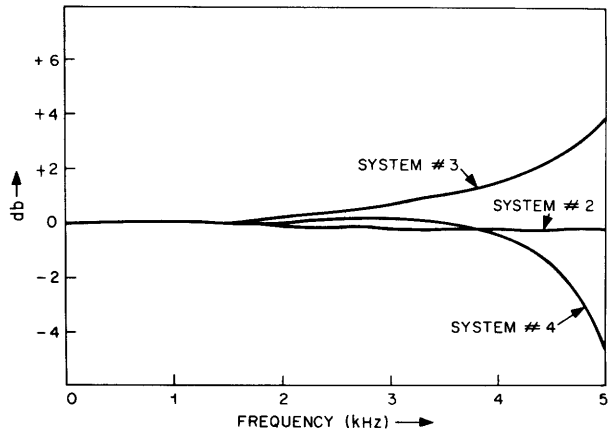

Fig. 11. Spectrum magnitude differences for IY.

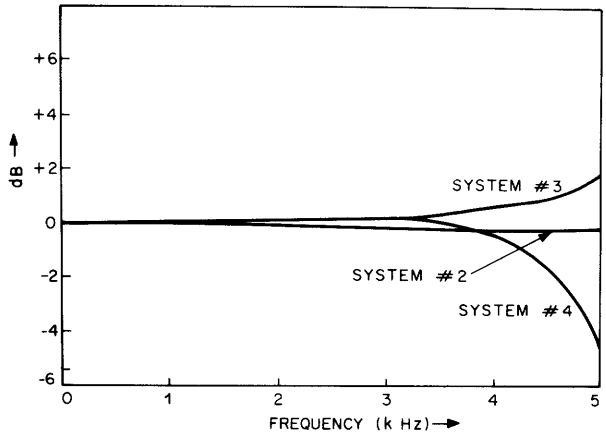

Fig. 12. Spectrum magnitude differences for A.

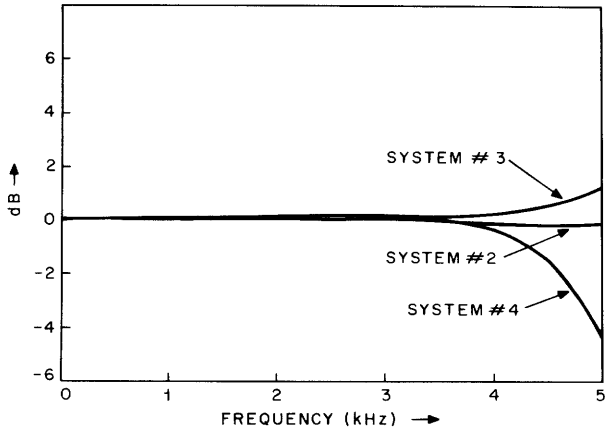

Fig. 13. Spectrum magnitude differences for OO.

increases the deviations of systems #2, #3, and #4 from the reference. Figure 14 shows the frequency responses of the two digital and one analog source filters. (We have included the differentiator as part of the source filter.) The plots are normalized so the peaks are set to 0 dB for all three cases. With the inclusion of source

Table 3. Peak difference between systems #4 and #1 for the vowels.

VOWEL	PEAK DIFFERENCE BETWEEN SYSTEMS #4 AND #1
IY	3.69 db
I	2.42
E	2.18
AE	2.00
UH	1.56
A	1.62
OW	1.44
U	1.25
OO	1.16
ER	0.65
AVERAGE	1.80 db

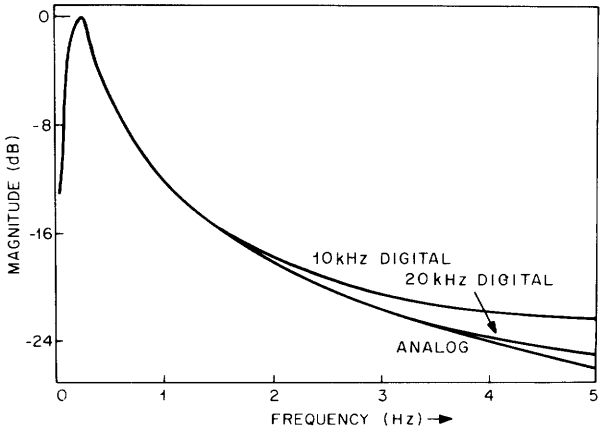

Fig. 14. Source filter characteristics.

filters the frequency response of system #2 is within 1 dB of the reference for all vowels and all frequencies. The peak difference, in the worst case, (for IY) between system #3 and the reference is 7.48 dB at 5 kHz. For all vowels except IY and for all frequencies below 4 kHz, the difference never exceeds 3.5 dB. It is possible that a digital source filter with slightly decreased bandwidth could bring the two results closer together.

IV. HIGHER POLE CORRECTION FOR THE ANALOG SYSTEM

The material to be presented here is incidental to the main line of development of this report and deals only with the question of the higher pole correction for analog formant synthesizers. The higher pole correction is used to approximate the higher modes of the vocal tract which are not explicitly present in the synthesizer. The frequency-response magnitude of this network (to be referred to as $Q(\omega)$) was derived by Gunnar Fant,[14] and is

$$|Q_k(\omega)| \cong e^{\frac{\omega^2}{\omega_1^2} R_k} \qquad (6)$$

with

$$R_k = \frac{\pi^2}{8} - \sum_{n=1}^{k} \frac{1}{(2n-1)^2},$$

in which it has been assumed that k analog formant networks are used to approximate the vocal tract, and ω_1 is the radian frequency of the first formant. In order to make $Q_k(\omega)$ into a network with fixed rather than variable parameters, ω_1 is usually chosen to be an average, say, $2\pi \times 500$ rps.

Our observations have been that the 5- and 10-pole analog synthesizers, both utilizing the $Q_k(\omega)$ specified by Eq. 6, nevertheless yielded substantially differing frequency-response curves. In fact, results were obtained which appeared to be qualitatively wrong. The result was that the 5-pole system was attenuated more with increasing frequency than the 10-pole system. Given that the 10-pole system utilized rather wide bandwidths for formants 6, 7, 8, 9, and 10 and that the higher pole correction presumably corrects for higher modes having narrower bandwidths, we should presume that the reverse result would have been observed. We conjectured that the approximations leading to Eq. 6 were too gross and, accordingly, we present a somewhat more refined formula for approximating the higher modes of the vocal tract for an analog formant synthesizer.

We begin with the assumptions used by Gunnar Fant in his original derivation: The vocal tract filter during vowels can be represented in the frequency domain by the infinite product

$$P(j\omega) = \prod_{n=1}^{\infty} \frac{s_n s_n^*}{(s-s_n)(s-s_n^*)}$$

$$= \prod_{n=1}^{k} \frac{\omega_n^2}{\left[\left(\omega_n^2-\omega^2\right)^2 + (2\sigma_n\omega)^2\right]^{1/2}} \prod_{n=k+1}^{\infty} \frac{\omega_n^2}{\left[\left(\omega_n^2-\omega^2\right)^2 + (2\sigma_n\omega)^2\right]^{1/2}}$$

$$= P_k(j\omega)\, Q_k(j\omega), \tag{7}$$

where σ_n and ω_n are the damping term and resonant frequency expressed in radians per second, and $P_k(j\omega)$ represents those k formants that are explicitly constructed in the synthesizer. Thus $Q_k(j\omega)$ appears as the product from k+1 to infinity of those formants that are not built into the synthesizer. To approximate $|Q_k(j\omega)|$, Gunnar Fant first assumes that σ_n is small enough to be set to zero for all n. This yields

$$|Q_k(j\omega)| = \prod_{n=k+1}^{\infty} \frac{1}{\left|1 - \frac{\omega^2}{\omega_n^2}\right|}, \tag{8}$$

and taking the logarithm of both sides, we obtain

$$\ln |Q_k(j\omega)| = -\sum_{n=k+1}^{\infty} \ln \left|1 - \frac{\omega^2}{\omega_n^2}\right|. \tag{9}$$

Gunnar Fant then expands the logarithm as a power in $(1/\omega_n)^2$ series and uses only the first two terms, which leads to Eq. 6. Our extension includes an extra term in this series, so that

$$\ln |Q_k(j\omega)| \approx \omega^2 \sum_{n=k+1}^{\infty} \frac{1}{\omega_n^2} + \frac{\omega^4}{2} \sum_{n=k+1}^{\infty} \frac{1}{\omega_n^4}. \tag{10}$$

If we now take the modes to be that of a straight pipe of length ℓ, the values of ω_n are periodic and are $\omega_n = (2n-1)\omega_1 = (2n-1)\frac{\pi c}{2\ell}$, where c is the velocity of sound. Making use of the identities $\frac{\pi^2}{8} = \sum_{n=1}^{\infty} \frac{1}{(2n-1)^2}$ and $\frac{\pi^4}{96} = \sum_{n=1}^{\infty} \frac{1}{(2n-1)^4}$, we arrive at

$$|Q_k(j\omega)| \approx e^{\left(\frac{\omega}{\omega_1}\right)^2 R_k + \frac{1}{2}\left(\frac{\omega}{\omega_1}\right)^4 L_k} \tag{11}$$

with

$$L_k = \frac{\pi^4}{96} - \sum_{n=1}^{k} \frac{1}{(2n-1)^4}.$$

The first term in Eq. 11 is the usual higher pole correction. Figure 15 shows plots of the first term of Eq. 11 (or Eq. 6) for the two cases k = 5 and k = 10. It is evident that both 5- and 10-pole systems need this standard higher pole correction.

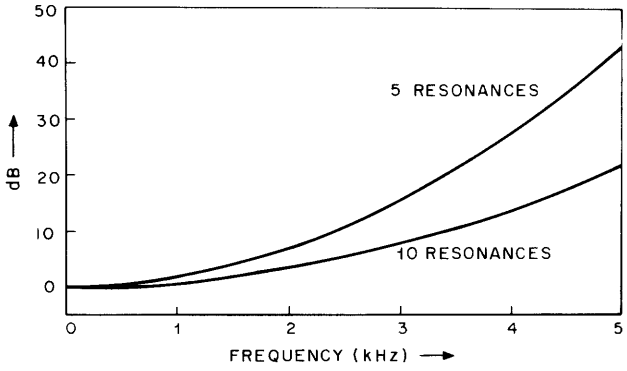

Fig. 15. First-order higher pole correction.

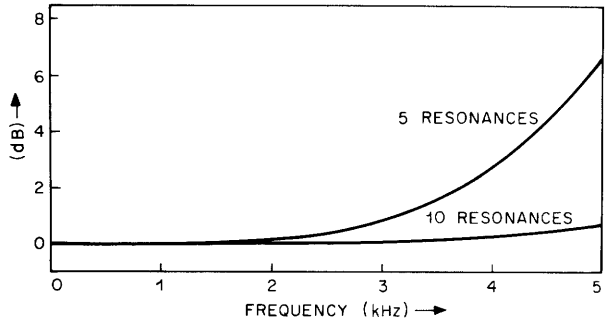

Fig. 16. Second-order improvement in higher pole correction.

Figure 16 shows plots of the second term in Eq. 11, namely, the expression $\exp\left[\frac{1}{2}\left(\frac{\omega}{\omega_1}\right)^4 L_k\right]$. We see that if a 10-pole synthesizer is used, this extra refinement is insignificant but if 5 poles are used, a reasonably significant correction is added. It should be noted that at frequencies above approximately 4 kHz the cross modes of the vocal tract are of significance. Thus the significance of this additional correction factor is diminished.

V. QUANTIZATION EFFECTS IN DIGITAL FORMANT SYNTHESIZERS

The finite length of the registers containing the signals flowing through the networks of Figs. 2 and 3 influences the results in several ways. First, the coefficients of the difference equation (2) cannot, in general, be specified exactly, so that the true pole positions may be in error. This is a fixed error and easily computed by comparing the quantized and nonquantized coefficient values. Second, the signals are perturbed by quantization during each iteration of the computation. If signal-level changes from one iteration to the next are large relative to an individual quantum step, then it seems reasonable to hypothesize[15, 2, 9, 10] that signal quantization behaves as additive noise, all such sources of noise are uncorrelated, and each sample of this noise is uncorrelated with past and future samples. Such a hypothesis greatly simplifies the formulation of the digital network quantization problem and makes it easier to interpret experimental results, but clearly there must first be some indication that valid predictions can be made on the basis of such a simple hypothesis. Therefore we shall first study the validity of the simple additive noise, and then discuss some of the results that have been obtained, these results being illuminated by reference to the model.

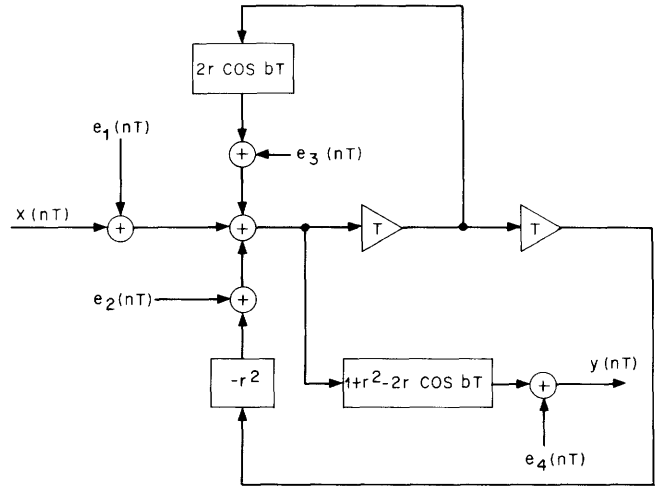

Fig. 17. Noise model formant network.

Figure 17 is a modified version of Fig. 3, wherein three noises e_1, e_2, and e_3 are added, corresponding to the round-off or truncation errors implicit in each of the three multiplications. We assume that each noise sample produced at every recursion is uncorrelated with all other noise samples produced by the same noise generator during other recursions, and that $e_1(nT)$, $e_2(nT)$, and $e_3(nT)$ are mutually uncorrelated even for the same iteration. Such an assumption is surely wrong if, for example, any two coefficients in the recursive equation were exactly equal, so that our hypothesis will not include such special cases. Thus all that needs to be known statistically are the

one-dimensional probability distributions associated with each of the three random variables. Again, a reasonable assumption is that e_1, e_2, and e_3 are uniformly distributed over a quantization interval and for fixed-point arithmetic, independent of signal level. We also specify that quantization levels be uniformly spaced (linear quantization of the signals). Whether or not the probability distributions depend on the sign of the signal is determined by the precise manner in which quantization is effected. Let us examine this point more closely.

In a digital computation, the product of two numbers can occupy a register of twice the length of each of the numbers. For example, the product of the two 5-bit positive binary numbers 0.1011 and 0.1110 yields the 10-bit product 00.100|11010. To store the result in a 5-bit register requires that the five lower bits be removed, and this may be accomplished via truncation, wherein the low-level bits (after a 1-bit left shift to restore the original decimal point placement) are simply removed, thereby yielding 0.1001. Alternatively, the result may be rounded-off to the nearest quantization level, to yield, in this example, the product 0.1010. Now, this last operation results in the uniform probability density shown in Fig. 18a, while Fig. 18b holds for truncation of a positive signal, and Fig. 18c holds for truncation of a negative signal. Thus, truncation introduces a quasi-periodic component of the resultant noise. If a sign-dependent truncation were performed which could lead to the result of either Fig. 18b or 18c regardless of signal sign, then only a DC component would be induced in the noise spectrum. The importance of raising these seemingly trivial points lies in the fact that different hardware configurations or different computer programs would be required, determined by how the extra bits were chopped off, and the programmer or designer ought to be cognizant of the effects of these different realizations on the resultant noise.

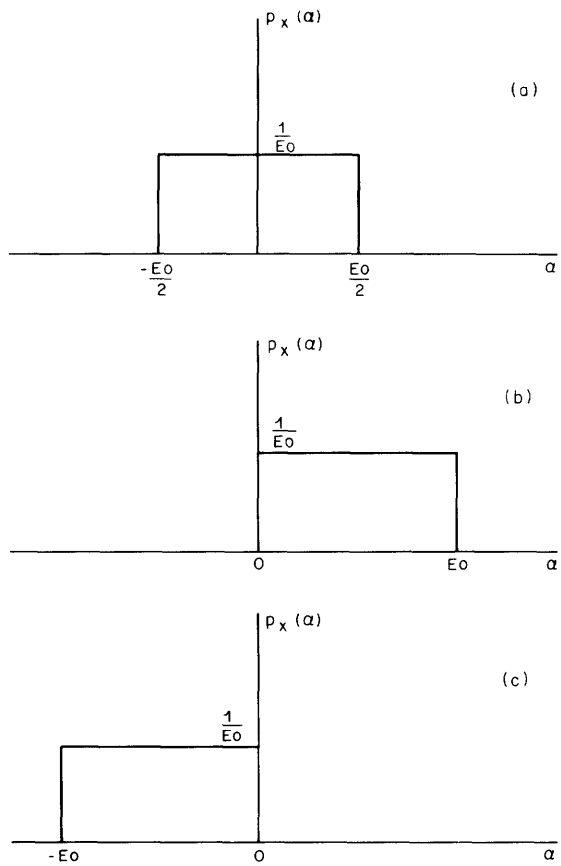

Fig. 18. Probability density functions of noise.

Returning now to the noise model of Fig. 17, let us consider the noise generated at the output of the digital filter caused, say, by $e_1(nT)$. The variance of this noise at any time nT created by a noise sample at m = 0 is given by $\sigma^2 h^2(nT)$, where σ^2 is the variance of $e_1(nT)$, and h(nT) is the network unit pulse

response. Similarly, the variance created by a noise sample at m = 1 is $\sigma^2 h^2(nT-T)$. Proceeding in this way, one can construct the formula for the output variance resulting from $e_1(nT)$ to be

$$\sigma_{d1}^2(nT) = \sigma^2 \sum_{m=0}^{n} h^2(mT). \tag{12}$$

This formulation has been explained in greater detail elsewhere.[2, 10]

The variance σ^2 of $e_1(nT)$ can be obtained by inspection of Fig. 18, and is $E_o^2/12$, where E_o is the magnitude of a single quantization step. To obtain the total variance caused by all of the noise sources indicated in Fig. 17, we need only add the contributions arising from each noise source; this yields

$$\sigma_d^2 = \sigma_{d1}^2 + \sigma_{d2}^2 + \sigma^2 = E_o^2/6 \left[\sum_{m=0}^{n} h^2(mT) + \frac{1}{2} \right]. \tag{13}$$

To obtain the total variance caused by all noise sources in a more complex network such as the 3 cascaded digital formant networks shown in Fig. 19, we add again the variances

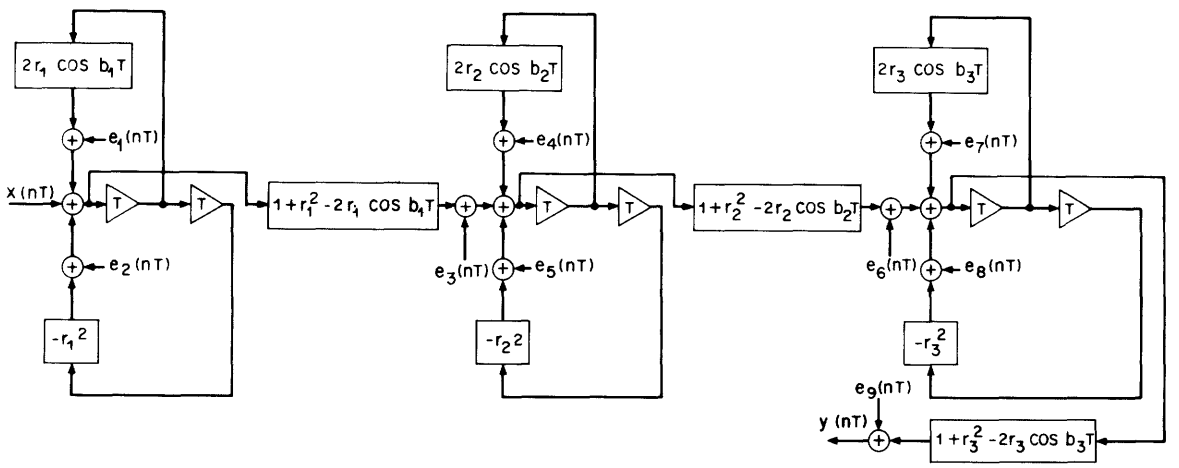

Fig. 19. Noise sources in a cascade of 3 formants.

resulting from each source, using that unit pulse response that describes the passage of that particular source through the system. For example, $e_1(nT)$ (Fig. 19) passes through all three digital networks, whereas $e_7(nT)$ passes through only the final one; thus, the h(nT) used to compute σ_{d1}^2 is different from the h(nT) used to compute σ_{d7}^2.

In a digital system wherein all poles are within the unit circle, the summation (12) converges to a finite value, so that, if we let the upper limit n of (12) become infinite, we have an expression for the "steady-state" variance of the system. Physically, one would expect this "steady state" to be reached in a time that is approximately the same

as the transient response time of the system. For this case, evaluation of (6) for specific networks is algebraically less cumbersome and, indeed, crude approximations can be made which increase physical insight into the noise effects and perhaps may help suggest improvements in configurations. Before further elaboration of these statements, let us first describe an experimental method of measuring the noise in an arbitrary system, and then show some results comparing theory with experiment which tend to verify our noise model.

The digital transfer function V(z) in Fig. 20 represents the complete 5-pole, 10-kHz formant synthesizer which we have described, including source and radiation transfer

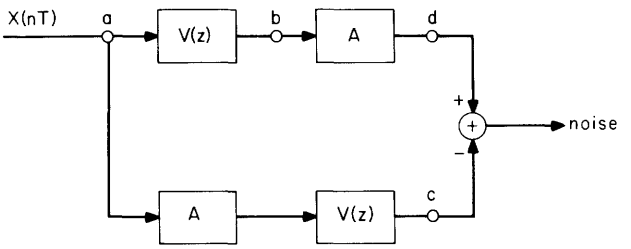

Fig. 20. Noise measurement on the digital formant synthesizer.

functions. A is an attenuator such that the output is a small fraction of the input, and x(nT) is a periodic train of pulses of 1 sampling interval duration. Since the amount of quantization noise is not a function of the input signal level, points b and c in Fig. 20 contain approximately equal noise levels. Attenuating the signal from b to d should not change the signal-to-noise ratio at these points; therefore, the noise at point c is appreciably larger than the noise at point d, although the signal levels are equal. Thus, subtracting the two signals should give a reasonable measure of the noise, especially if significant noise is present.

In order to compare theory and experiment, the noise variance from V(z) should be measured by using the arrangement in Fig. 20, and this result should be compared with that obtained by application of Eq. 12 to the same system. We did this for the 10 vowels listed in Table 1. The variance was measured by averaging the sum of the squares of 3500 samples of the noise. Measurements showed that the noise had zero mean. The precise cascading of the components of V(z) is shown in Fig. 6. The wrong value of the damping term for the source filter was inadvertantly used in this experiment (60 Hz instead of 250 Hz), but this should have no effect on the general validity of this comparison between theory and fact. Comparisons of the variances, expressed as octal numbers, are shown in Table 4. Although the agreement is not perfect, it is clearly close enough to encourage use of our simple noise model.

We now can return to the problem of crudely approximating the noise generated by a single digital formant. With the use of the result[10]

$$\sum_{n=0}^{\infty} h^2(nT) = \frac{1}{2\pi j} \oint H(z)\, H(1/z)\, z^{-1}\, dz, \tag{14}$$

where H(z) and h(nT) is a transform pair and the integral is around the unit circle, computation of Eq. 12 is easily performed by using the calculus of residues if H(z) is a

Table 4. Comparison of theory and experiment for predicting noise.

VOWEL	MEASURED NOISE	THEORETICALLY DETERMINED VALUE
IY	702,664	735,547
I	125,574	114,717
E	101,110	104,036
AE	57,674	52,241
UH	51,414	52,241
A	51,050	55,346
OW	50,700	52,763
U	53,460	52,242
OO	41,044	42,123
ER	27,574	27,465

digital formant network. The approximate result obtained when the poles are close to the unit circle is $E_o^2/12\epsilon$, where $\epsilon = 1 - r$. Since the gain at resonance of a digital formant network is also inversely proportional to ϵ, it follows that a network will amplify the noise proportionally to its resonance gain. From this it follows that the noise generated by the digital formant network can be altered by rearrangement of the order of the chain. For example, since F_5 has a higher resonance gain than F_1, it should appear earlier in the chain because thereby all of the noise generated by the system following F_5 does not pass through F_5 and is not amplified as much.

We see that when using a simple noise model quantization considerations help us decide how the synthesizer is to be arranged, and in what order the formant networks should be arranged to keep the noise low. Other considerations also enter into such decisions. For example, it has been conjectured that the system is less sensitive to transient disturbances following formant frequency changes if the higher formant networks precede the lower ones. Intuitively, this argument resembles the noise argument and leads to the same or similar arrangement. Another consideration is dynamic

range; the problems arising here are equivalent to those arising in analog systems wherein the formants are arranged so that the signal becomes neither too large nor too small. The comparisons in Figs. 2 and 3 allude to this problem.

A further benefit may be derived by closer examination of the precise way in which the computation for a single digital formant is carried out. Often, the way the computation is performed depends on the computer; in the sequel we shall illustrate by an

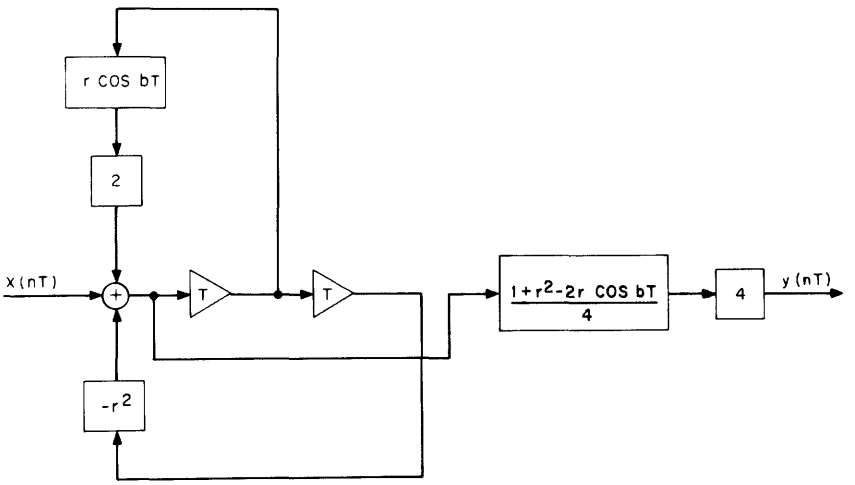

Fig. 21. One way of realizing a digital formant on TX-2 computer.

example, using a TX-2 computer program. The TX-2 is a fixed-point computer with an automatic left shift after multiplication so that if the decimal points directly follow the high-level bit (as in the example already given), then the product will automatically have the same decimal point position. This makes it convenient to treat all numbers as decimal fractions. The coefficient 2r cos (bT) in Eq. 2 is usually greater than unity, however, and the program must take this into account. Two ways of doing this are illustrated in Figs. 21 and 22. Multiplications by powers of two are only shifts, of course, so that the restriction of treating numbers as decimal fractions does not apply. We intuitively feel that the configuration of Fig. 21 leads to better signal-to-noise ratio, since the round-off or truncation caused by the multiplications in either case is the same but the signal levels in Fig. 21 are maintained higher. Experimental results indicate that the noise variance of the formant network by using Fig. 21 is approximately double that obtained by using Fig. 22.

Finally, we present experimental results that make it possible to specify the required register lengths needed for each of the data-carrying registers in each of the networks. This is accomplished in the following way: A given vowel is generated by setting formants 1, 2, and 3 to one of the rows of values in Table 1; the digital synthesizer is excited by a periodic pulse train corresponding to the pitch (for most experiments the pitch was set to 125 Hz), and the magnitude of this excitation is systematically

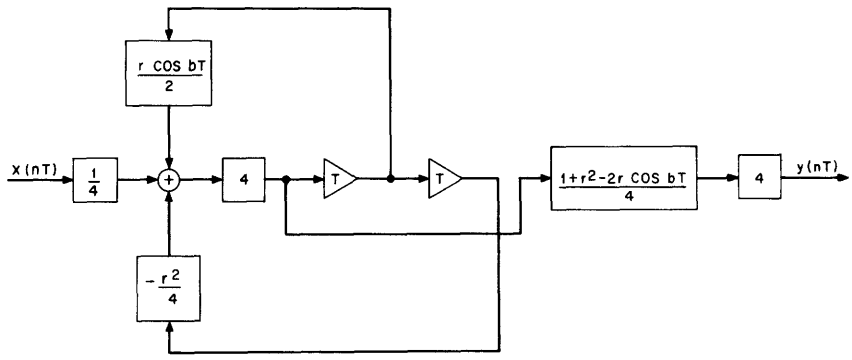

Fig. 22. Alternative method of realizing a digital formant on TX-2 computer.

reduced until the effects of quantization are audible. Also, the signal-to-noise ratio (defined as the ratio of the rms of the output signal to the rms value of the noise) is measured. During the execution of the program, peak magnitudes are recorded for each register in the system. From this information, it is possible to construct a table for any given configuration listing the number of bits needed for each register. Referring to Figs. 2 and 3, we see that only two registers per digital formant need be listed, for example, in Fig. 2, the input and output of the numerator multiplier. The registers containing y(nT-T) and y(nT-2T) will be of the same length as the register containing y(nT).

For convenience, we express each digital formant H(z) as the ratio N(z)/D(z). The chain drawn in Fig. 23 shows the sequence of operations in one particular run. Note that we have omitted the numerator factors N_5, N_4, and N_0. These are fixed multipliers, and should not be included, since they introduce extraneous and unnecessary noise.

Table 5 shows the required register length associated with each member of the chain. The particular ordering of the chain was chosen to try to pass as little noise as possible through the high-gain formants; hence, F_5 and F_4 were put at the beginning. The signal-to-noise ratio, defined as the rms signal divided by the rms noise, is listed in the last column of Table 5, in bits. Thus, for example, 8 bits corresponds to a ratio of

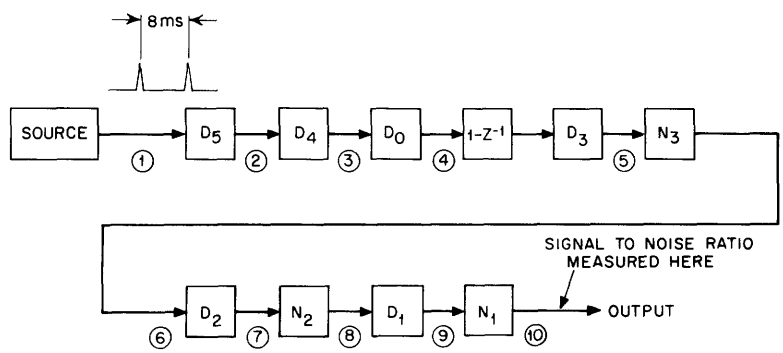

Fig. 23. The 540321 sequence of digital formants.

Table 5. Register lengths for 540321 synthesizer configuration.

	NODE #										
VOWEL	1	2	3	4	5	6	7	8	9	10	S/N
IY	10	12	13	11	12	14	13	14	13	8	4.5
I	10	12	13	11	12	13	12	12	12	8	4
E	10	12	13	11	12	12	12	12	12	9	4.5
AE	10	12	13	11	11	12	11	11	11	9	4
UH	10	12	13	11	11	12	11	10	11	8	5
A	10	12	13	11	11	12	11	10	11	9	4.5
OW	10	12	13	11	11	12	11	9	12	9	4
U	10	12	13	11	11	12	11	10	11	7	4
OO	10	12	13	11	11	12	11	9	12	7	4
ER	10	12	13	11	11	11	11	10	12	8	4
Maximum over all vowels	10	12	13	11	12	14	13	14	13	9	

256, while $8\frac{1}{2}$ bits is $\sqrt{512}$. Listeners agreed that this configuration corresponded most closely to the threshold of audible noise. Speaking rather loosely, if we allow a reasonable tolerance for problems such as transients caused by formant changes, it would seem that a computer with an 18-bit register length would satisfy fidelity requirements on a digital formant synthesizer.

We should keep in mind that the numbers obtained hold for a 5-pole, 10-kHz system. If the number of poles is increased, the situation worsens. More noise is generated and the problem of maintaining fairly uniform dynamic range becomes more difficult. If the sampling rate is increased, the situation also worsens, since the poles come closer to the unit circle, so that the gain of the system increases. Again, this means that it becomes more difficult to uniformly distribute register lengths, although the effect on the signal-to-noise ratio is not clear.

In contrast to the configuration of Fig. 23, where gains were judiciously adjusted, Fig. 24 and Table 6 show the result of a rather arbitrary arrangement of formants. Notice that although the register lengths need to be larger in this case, comparable signal-to-noise ratio results. Thus, we see that some care in the ordering of the elements results in a more efficient system, and may make the difference between

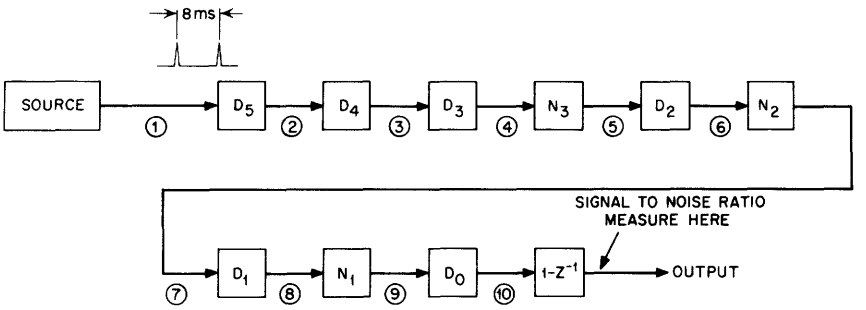

Fig. 24. The 543210 sequence of digital formants.

Table 6. Register lengths for 543210 synthesizer configuration.

	NODE #										
VOWEL	1	2	3	4	5	6	7	8	9	10	S/N (bits)
IY	12	14	15	15	16	16	17	15	10	12	5
I	12	14	15	14	15	15	15	14	10	12	5
E	12	14	15	14	15	14	15	14	10	12	5
AE	12	14	15	14	15	14	14	13	11	12	5
UH	12	14	15	14	15	14	13	12	9	12	5½
A	12	14	15	14	15	14	13	12	10	13	5
OW	12	14	15	14	15	13	12	12	9	12	4
U	12	14	15	14	15	13	12	12	8	12	4½
OO	12	14	15	14	15	13	11	12	7	12	4½
ER	12	14	15	13	13	13	12	13	9	12	5
Maximum over all vowels	12	14	15	15	16	16	17	15	10	13	

successful and unsuccessful runs on an 18-bit computer.

For each digital resonator there are 3 noise sources corresponding to the 3 multipliers. We have discussed a method of reducing the number of multipliers by one, for the fixed resonators, by removing the numerator multiplier. This method cannot be used, however, for the variable formants because the numerator contains terms depending on the frequency of the resonator. A method for reducing the number of multipliers to two per formant for both variable and fixed formants has been suggested by C. H. Coker. Figure 25 shows this method of realizing a digital formant. Differences of the input signal and delayed versions of the output signal are the multiplier inputs, thereby eliminating the output multiplier.

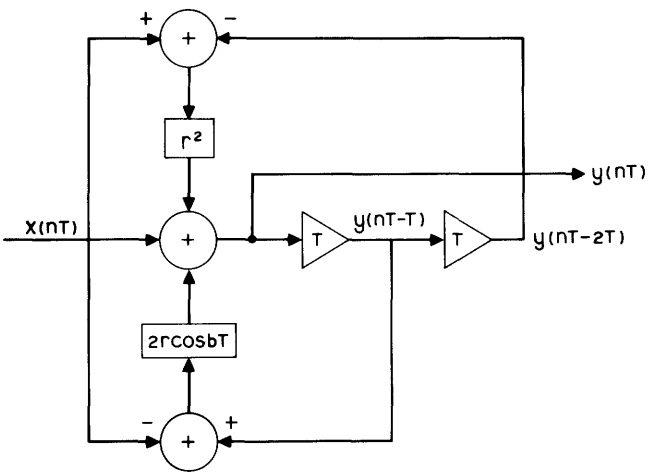

Fig. 25. Digital formant with 2 multipliers.

One would expect the noise variance at the output of the formant network of Fig. 25 to be approximately two-thirds the noise variance of Fig. 3. This is not the case, however. The noise variance at the output node of Fig. 25 is identical to the noise variance at the output of the summer of Fig. 3, since in both cases the comparable noises go through identical loops. The noise of Fig. 3 is then multiplied by the numerator coefficient which, for frequencies less than 1667 Hz, is less than one in magnitude. Hence the noise of Fig. 3 can be less than the noise of Fig. 25 by an appreciable amount.

The formant network of Fig. 25 was used in Fig. 23 to replace formants 1, 2, and 3 (the low-gain formants), and signal-to-noise ratios were measured and compared with those used in the network of Fig. 3. The results are presented in Table 7. The first column shows the signal-to-noise ratio (in bits) for the network of Fig. 25, and the second column shows signal-to-noise ratios for the network of Fig. 3. The signal-to-noise ratios are from $\frac{1}{2}$ bit to 3 bits lower when using the network of Fig. 25. Even for the high-gain formants (F_4 and F_5) the network of Fig. 25 provides no advantages over the network of Fig. 3. This is because we

Table 7. Comparison of two formant networks.

VOWEL	I S/N (bits)	II S/N (bits)
IY	2	4½
I	2½	4
E	3	4½
AE	3½	4
UH	3½	5
A	3½	4½
OW	2½	4
U	2	4
OO	1	4
ER	3	4

Table 8. Noise variance in bits as a function of input level for the synthesizer of Figure 23.

INPUT LEVEL (bits)	VOWEL IY	I	E	AE	UH	A	OW	U	OO	ER
9	2	2	3	3	2	4	5	3	1	3
10	1	3	2	3	2	3	3	2	1	3
11	2	2	2	3	3	5	3	3	2	2
12	2	3	4	4	4	6	6	3	3	4
13	2	3	4	3	4	5	4	3	2	4
15	1	2	2	2	3	4	3	2	2	4
16	2	3	3	3	4	5	5	3	3	3
17	2	2	2	4	4	5	4	2	2	4
18	2	2	2	3	3	5	4	4	2	3
19	2	4	3	4	3	6	4	4	4	4

do not have to use the high-gain numerator multiplier for these fixed formants. Therefore, the internal noise generated by both networks is identical. But the network of Fig. 25 automatically includes the high-gain multiplier; therefore, the noise at the input to the network (as well as the signal) will be amplified. This is an undesirable feature when you are trying to keep register lengths uniform.

Experimental study of the noise generated by a digital formant synthesizer showed that this noise was correlated both with the pitch and the vowel; so much so that one could detect by eye the pitch period from the noise waveform, and hear the vowel when listening to the noise.

The dependence of the noise variance upon input level was investigated quantitatively by using the synthesizer of Fig. 23. The results of this investigation are presented in Table 8. For any one vowel the noise variance depends upon the input level, but not in a smooth, continuous way. The peak variation in noise variance (in bits) for any one vowel was 3 bits. Table 8 indicates a fairly significant variation of noise variance with signal level. This variation is greater than would have been expected from Table 4. This is possibly due to the low noise levels of the data of Table 8. The agreement between theory and experiment may be better when a significant amount of noise is generated – as is the case for the data of Table 4.

Acknowledgment

This work was carried out in the Speech Communication Group of the Research Laboratory of Electronics, whose work was supported in part by the U. S. Air Force Cambridge Research Laboratories (Office of Aerospace Research) under Contract AF19(628)-5661, and in part by the National Institutes of Health (Grant 5 RO1 NB-04332-05). Dr. Rabiner also received support from a National Science Foundation Fellowship, June 1964–September 1966.

Dr. Bernard Gold was on leave, September 1965–June 1966, from Lincoln Laboratory, a center for research operated by the Massachusetts Institute of Technology with the support of the U. S. Air Force, as a Visitor in the Speech Communication Group of the Research Laboratory of Electronics. He subsequently returned to Lincoln Laboratory.

Dr. Rabiner is now associated with Bell Telephone Laboratories, Murray Hill, New Jersey.

The authors wish to express their appreciation to Professor Kenneth N. Stevens, of the Speech Communication Group of R. L. E., for his interest in this work; also to Lincoln Laboratory, M. I. T., for the use of their TX-2 computer, and to Bell Telephone Laboratories, Incorporated, for preparing the figures which were used in this report.

References

1. J. F. Kaiser and F. Kuo (eds.), System Analysis by Digital Computer (John Wiley and Sons, Inc., New York, 1966).
2. C. M. Rader and B. Gold, "Digital Filter Design Techniques in the Frequency Domain," Proc. IEEE 55, 149-171 (1967).
3. J. L. Flanagan, C. H. Coker, and C. M. Bird, "Digital Computer Simulation of a Formant-Vocoder Speech Synthesizer," 15th Annual Meeting of the Audio Engineering Society, 1963.
4. L. R. Rabiner, "Speech Synthesis by Rule: An Acoustic Domain Approach," Ph. D. Thesis, Department of Electrical Engineering, Massachusetts Institute of Technology, Cambridge, Mass., May 1967.
5. J. L. Flanagan, Speech Analysis Synthesis and Perception (Academic Press Inc., New York, 1965).
6. G. Fant and J. Martony, "Speech Synthesis," Quarterly Progress Report, Speech Transmission Laboratory, University of Stockholm, July 1962.
7. R. S. Tomlinson, "SPASS – An Improved Terminal-Analog Speech Synthesizer," J. Acoust. Soc. Am. 38, 940 (1965) (A).
8. J. F. Kaiser, "Some Practical Considerations in the Realization of Linear Digital Filters," Proc. Third Allerton Conference, 1965, pp. 621-633.
9. J. B. Knowles and R. Edwards, "Effect of a Finite-Word-Length Computer in a Sampled-Data Feedback System," Proc. Inst. Elec. Engrs. (London), Vol. 112, pp. 1197-1207, June 1965.
10. B. Gold and C. M. Rader, "Effects of Quantization Noise in Digital Filters," Proc. Spring Joint Computer Conference, 1966, pp. 213-219.
11. G. Peterson and H. Barney, "Control Methods Used in a Study of the Vowels," J. Acoust. Soc. Am. 24, 175-184 (1952).
12. H. Dunn, "Methods of Measuring Vowel Formant Bandwidths," J. Acoust. Soc. Am. 33, 1737-1746 (1961).
13. G. Fant, Acoustic Theory of Speech Production (Mouton and Co., s' Gravenhage, 1960).
14. Ibid.
15. W. R. Bennett, "Spectra of Quantized Signals," Bell System Tech. J. 27, 446-472 (July 1948).

UNCLASSIFIED

Security Classification

DOCUMENT CONTROL DATA - R & D

(Security classification of title, body of abstract and indexing annotation must be entered when the overall report is classified)

1. ORIGINATING ACTIVITY *(Corporate author)*

Research Laboratory of Electronics
Massachusetts Institute of Technology
Cambridge, Massachusetts 02139

2a. REPORT SECURITY CLASSIFICATION

Unclassified

2b. GROUP

3. REPORT TITLE

Analysis of Digital and Analog Formant Synthesizers

4. DESCRIPTIVE NOTES *(Type of report and inclusive dates)*

Technical Report

5. AUTHOR(S) *(First name, middle initial, last name)*

Bernard Gold
Lawrence R. Rabiner

6. REPORT DATE	7a. TOTAL NO. OF PAGES	7b. NO. OF REFS
June 28, 1968	42	15

8a. CONTRACT OR GRANT NO.	9a. ORIGINATOR'S REPORT NUMBER(S)
DA 28-043-AMC-02536(E)	Technical Report 465
b. PROJECT NO. 200-14501-B31F	
c.	9b. OTHER REPORT NO(S) *(Any other numbers that may be assigned this report)*
d.	None

10. DISTRIBUTION STATEMENT

Distribution of this report is unlimited.

11. SUPPLEMENTARY NOTES	12. SPONSORING MILITARY ACTIVITY
	Joint Services Electronics Program thru USAECOM, Fort Monmouth, N. J.

13. ABSTRACT

A digital formant is a resonant network based on the dynamics of second-order linear difference equations. A serial chain of digital formants can approximate the vocal tract during vowel production. The digital formant is defined and its properties are discussed, using z-transform notation. The results of detailed frequency response computations of both digital and conventional 'analog' formant synthesizers are then presented. These results indicate that the digital system without higher pole correction is a closer approximation than the analog system with higher pole correction. A set of measurements on the signal and noise properties of the digital system is described. Synthetic vowels generated for different signal-to-noise ratios help specify the required register lengths for the digital realization. A comparison between theory and experiment is presented.

DD FORM 1 NOV 65 1473 (PAGE 1)

S/N 0101-807-6811

UNCLASSIFIED

Security Classification

A-31408

14. KEY WORDS	LINK A		LINK B		LINK C	
	ROLE	WT	ROLE	WT	ROLE	WT
digital formant						
higher pole correction						
formant synthesizer						
digital filter						
finite register length						
quantization noise						
round-off errors						

JOINT SERVICES ELECTRONICS PROGRAM
REPORTS DISTRIBUTION LIST

Department of Defense

Dr. A. A. Dougal
Asst Director (Research)
Ofc of Defense Res & Eng
Department of Defense
Washington, D. C. 20301

Office of Deputy Director
(Research and Information, Room 3D1037)
Department of Defense
The Pentagon
Washington, D. C. 20301

Director
Advanced Research Projects Agency
Department of Defense
Washington, D. C. 20301

Director for Material Sciences
Advanced Research Projects Agency
Department of Defense
Washington, D. C. 20301

Headquarters
Defense Communications Agency (333)
The Pentagon
Washington, D. C. 20305

Defense Documentation Center
Attn: TISIA
Cameron Station, Bldg. 5
Alexandria, Virginia 22314

Director
National Security Agency
Attn: Librarian C-332
Fort George G. Meade, Maryland 20755

Weapons Systems Evaluation Group
Attn: Col. Daniel W. McElwee
Department of Defense
Washington, D. C. 20305

Director
National Security Agency
Fort George G. Meade, Maryland 20755
Attn: Mr. James Tippet
R 3/H20

Central Intelligence Agency
Attn: OCR/DD Publications
Washington, D. C. 20505

Department of the Air Force

Colonel Kee
AFRSTE
Hqs. USAF
Room ID-429, The Pentagon
Washington, D. C. 20330

Aerospace Medical Division
AMD (AMRXI)
Brooks Air Force Base, Texas 78235

AUL3T-9663
Maxwell Air Force Base, Alabama 36112

AFFTC (FTBPP-2)
Technical Library
Edwards Air Force Base, California 93523

AF Unit Post Office
Attn: SAMSO (SMSDI-STINFO)
Los Angeles, California 90045

Lt. Col. Charles M. Waespy
Hq USAF (AFRDSD)
The Pentagon
Washington, D. C. 20330

SSD (SSTRT/Lt. Starbuck)
AFUPO
Los Angeles, California 90045

Det #6, OAR (LOOAR)
Air Force Unit Post Office
Los Angeles, California 90045

Systems Engineering Group (RTD)
Technical Information Reference Branch
Attn: SEPIR
Directorate of Engineering Standards
& Technical Information
Wright-Patterson Air Force Base,
Ohio 45433

ARL (ARIY)
Wright-Patterson Air Force Base,
Ohio 45433

Dr. H. V. Noble
Air Force Avionics Laboratory
Wright-Patterson Air Force Base,
Ohio 45433

Mr. Peter Murray
Air Force Avionics Laboratory
Wright-Patterson Air Force Base,
Ohio 45433

AFAL (AVTE/R. D. Larson)
Wright-Patterson Air Force Base,
Ohio 45433

Commanding General
Attn: STEWS-WS-VT
White Sands Missile Range,
New Mexico 88002

RADC (EMLAL-1)
Griffiss Air Force Base, New York 13442
Attn: Documents Library

Academy Library (DFSLB)
U. S. Air Force Academy
Colorado Springs, Colorado 80912

Mr. Morton M. Pavane, Chief
AFSC STLO (SCTL-5)
26 Federal Plaza, Room 1313
New York, New York 10007

Lt. Col. Bernard S. Morgan
Frank J. Seiler Research Laboratory
U. S. Air Force Academy
Colorado Springs, Colorado 80912

APGC (PGBPS-12)
Eglin Air Force Base, Florida 32542

AFETR Technical Library
(ETV, MU-135)
Patrick Air Force Base, Florida 32925

AFETR (ETLLG-1)
STINFO Office (for Library)
Patrick Air Force Base, Florida 32925

Dr. L. M. Hollingsworth
AFCRL (CRN)
L. G. Hanscom Field
Bedford, Massachusetts 01731

AFCRL (CRMXLR)
AFCRL Research Library, Stop 29
L. G. Hanscom Field
Bedford, Massachusetts 01731

Colonel Robert E. Fontana
Department of Electrical Engineering
Air Force Institute of Technology
Wright-Patterson Air Force Base,
Ohio 45433

Mr. Billy Locke
Plans Directorate
USAF Security Service
Kelly Air Force Base, Texas 78241

Colonel A. D. Blue
RTD (RTTL)
Bolling Air Force Base, D. C. 20332

Dr. I. R. Mirman
AFSC (SCT)
Andrews Air Force Base, Maryland 20331

AFSC (SCTR)
Andrews Air Force Base, Maryland 20331

Lt. Col. J. L. Reeves
AFSC (SCBB)
Andrews Air Force Base, Maryland 20331

ESD (ESTI)
L. G. Hanscom Field
Bedford, Massachusetts 01731

AEDC (ARO, INC)
Attn: Library/Documents
Arnold Air Force Station, Tennessee 37389

European Office of Aerospace Research
Shell Building
47 Rue Cantersteen
Brussels, Belgium

Lt. Col. Robert B. Kalisch (SREE)
Chief, Electronics Division
Directorate of Engineering Sciences
Air Force Office of Scientific Research
Arlington, Virginia 22209

Mr. H. E. Webb (EMIA)
Rome Air Development Center
Griffiss Air Force Base, New York 13442

Department of the Army

U. S. Army Research Office
Attn: Physical Sciences Division
3045 Columbia Pike
Arlington, Virginia 22204

Research Plans Office
U. S. Army Research Office
3045 Columbia Pike
Arlington, Virginia 22204

Lt. Col. Richard Bennett
AFRDDD
The Pentagon
Washington, D. C. 20301

Weapons Systems Evaluation Group
Attn: Colonel John B. McKinney
400 Army-Navy Drive
Arlington, Virginia 22202

Colonel H. T. Darracott
Advanced Materiel Concepts Agency
U.S. Army Materiel Command
Washington, D. C. 20315

Commanding General
U.S. Army Materiel Command
Attn: AMCRD-TP
Washington, D. C. 20315

Commanding General
U.S. Army Communications Command
Fort Huachuca, Arizona 85163

Commanding Officer
U.S. Army Materials Research Agency
Watertown Arsenal
Watertown, Massachusetts 02172

Commanding Officer
U.S. Army Ballistics Research Laboratory
Attn: V. W. Richards
Aberdeen Proving Ground
Aberdeen, Maryland 21005

Commandant
U.S. Army Air Defense School
Attn: Missile Sciences Division, C&S Dept.
P. O. Box 9390
Fort Bliss, Texas 79916

Commanding General
U.S. Army Missile Command
Attn: Technical Library
Redstone Arsenal, Alabama 35809

Commanding General
Frankford Arsenal
Attn: SMUFA-L6000-64-4 (Dr. Sidney Ross)
Philadelphia, Pennsylvania 19137

U.S. Army Munitions Command
Attn: Technical Information Branch
Picatinney Arsenal
Dover, New Jersey 07801

Commanding Officer
Harry Diamond Laboratories
Attn: Dr. Berthold Altman (AMXDO-TI)
Connecticut Avenue and Van Ness St. N.W.
Washington, D. C. 20438

Commanding Officer
U.S. Army Security Agency
Arlington Hall
Arlington, Virginia 22212

Commanding Officer
U.S. Army Limited War Laboratory
Attn: Technical Director
Aberdeen Proving Ground
Aberdeen, Maryland 21005

Commanding Officer
Human Engineering Laboratories
Aberdeen Proving Ground
Aberdeen, Maryland 21005

Director
U.S. Army Engineer
Geodesy, Intelligence and Mapping
Research and Development Agency
Fort Belvoir, Virginia 22060

Commandant
U.S. Army Command and General
Staff College
Attn: Secretary
Fort Leavenworth, Kansas 66270

Dr. H. Robl, Deputy Chief Scientist
U.S. Army Research Office (Durham)
Box CM, Duke Station
Durham, North Carolina 27706

Commanding Officer
U.S. Army Research Office (Durham)
Attn: CRD-AA-IP (Richard O. Ulsh)
Box CM, Duke Station
Durham, North Carolina 27706

Librarian
U.S. Army Military Academy
West Point, New York 10996

The Walter Reed Institute of Research
Walter Reed Medical Center
Washington, D.C. 20012

U.S. Army Mobility Equipment Research
and Development Center
Attn: Technical Document Center
Building 315
Fort Belvoir, Virginia 22060

Commanding Officer
U.S. Army Electronics R&D Activity
White Sands Missile Range,
New Mexico 88002

Mr. Norman J. Field (AMSEL-RD-S)
Chief, Office of Science and Technology
U.S. Army Electronics Command
Fort Monmouth, New Jersey 07703

Mr. Robert O. Parker
Exec. Secretary, JSEP
U.S. Army Electronics Command
AMSEL-RD-S (Rm. 2D-113A)
Fort Monmouth, New Jersey 07703

Commanding General
U.S. Army Electronics Command
Fort Monmouth, New Jersey 07703
Attn: AMSEL-SC
RD-D
RD-G
RD-GF
RD-MAT
XL-D
XL-E
XL-C
XL-S
HL-D
HL-CT-R
HL-CT-P
HL-CT-L
HL-CT-O
HL-CT-I
HL-CT-A
NL-D
NL-A
NL-P
NL-R
NL-S
KL-D
KL-E
KL-S
KL-TM
KL-TQ
KL-TS
VL-D
WL-D

Department of the Navy

Chief of Naval Research
Department of the Navy
Washington, D. C. 20360
Attn: Code 427

Naval Electronics Systems Command
ELEX 03
Falls Church, Virginia 22046

Naval Ship Systems Command
SHIP 031
Washington, D. C. 20360

Naval Ship Systems Command
SHIP 035
Washington, D. C. 20360

Naval Ordnance Systems Command
ORD 32
Washington, D. C. 20360

Naval Air Systems Command
AIR 03
Washington, D. C. 20360

Commanding Officer
Office of Naval Research Branch Office
Box 39, Navy No 100 F.P.O.
New York, New York 09510

Commanding Officer
Office of Naval Research Branch Office
219 South Dearborn Street
Chicago, Illinois 60604

Commanding Officer
Office of Naval Research Branch Office
1030 East Green Street
Pasadena, California 91101

Commanding Officer
Office of Naval Research Branch Office
207 West 24th Street
New York, New York 10011

Commanding Officer
Office of Naval Research Branch Office
495 Summer Street
Boston, Massachusetts 02210

Director, Naval Research Laboratory
Technical Information Officer
Washington, D. C. 20360
Attn: Code 2000

Commander
Naval Air Development and Material Center
Johnsville, Pennsylvania 18974

Librarian
U.S. Naval Electronics Laboratory
San Diego, California 95152

Commanding Officer and Director
U.S. Naval Underwater Sound Laboratory
Fort Trumbull
New London, Connecticut 06840

Librarian
U.S. Navy Post Graduate School
Monterey, California 93940

Commander
U.S. Naval Air Missile Test Center
Point Mugu, California 93041

Director
U.S. Naval Observatory
Washington, D. C. 20390

Chief of Naval Operations
OP-07
Washington, D. C. 20350

Director, U.S. Naval Security Group
Attn: G43
3801 Nebraska Avenue
Washington, D. C. 20390

Commanding Officer
Naval Ordnance Laboratory
White Oak, Maryland 21502

Commanding Officer
Naval Ordnance Laboratory
Corona, California 91720

Commanding Officer
Naval Ordnance Test Station
China Lake, California 93555

Commanding Officer
Naval Avionics Facility
Indianapolis, Indiana 46241

Commanding Officer
Naval Training Device Center
Orlando, Florida 32811

U.S. Naval Weapons Laboratory
Dahlgren, Virginia 22448

U.S. Naval Applied Science Laboratory
Flushing and Washington Avenues
Brooklyn, New York 11251
Attn: Mr. Robert Schwartz, Code 926

W. A. Eberspacher
Technical Consultant - System Integration
Code 5340A, Box 15
Naval Missile Center
Point Mugu, California 93041

Weapons Systems Test Division
Naval Air Test Center
Patuxtent River, Maryland 20670
Attn: Library

Head, Technical Division
U.S. Naval Counter Intelligence
Support Center
Fairmont Building
4420 North Fairfax Drive
Arlington, Virginia 22203

Other Government Agencies

Mr. Charles F. Yost
Special Assistant to the Director
of Research
National Aeronautics and
Space Administration
Washington, D. C. 20546

Dr. H. Harrison, Code RRE
Chief, Electrophysics Branch
National Aeronautics and
Space Administration
Washington, D. C. 20546

Goddard Space Flight Center
National Aeronautics and
Space Administration
Attn: Library C3/TDL
Green Belt, Maryland 20771

NASA Lewis Research Center
Attn: Library
21000 Brookpark Road
Cleveland, Ohio 44135

National Science Foundation
Attn: Program Director
Engineering Systems Program, ENG
1800 G. Street, N. W.
Washington, D. C. 20550

U.S. Atomic Energy Commission
Division of Technical Information Extension
P. O. Box 62
Oak Ridge, Tennessee 37831

Los Alamos Scientific Laboratory
Attn: Reports Library
P. O. Box 1663
Los Alamos, New Mexico 87544

NASA Scientific & Technical Information
Facility
Attn: Acquisitions Branch (S/AK/DL)
P. O. Box 33
College Park, Maryland 20740

NASA, Langley Research Center
Langley Station
Hampton, Virginia 23365
Attn: Mr. R. V. Hess, Mail Stop 160

Non-Government Agencies

Director
Research Laboratory of Electronics
Massachusetts Institute of Technology
Cambridge, Massachusetts 02139

Polytechnic Institute of Brooklyn
55 Johnson Street
Brooklyn, New York 11201
Attn: Mr. Jerome Fox
Research Coordinator

Director
Columbia Radiation Laboratory
Columbia University
538 West 120th Street
New York, New York 10027

Director
Coordinated Science Laboratory
University of Illinois
Urbana, Illinois 61803

Director
Stanford Electronics Laboratories
Stanford University
Stanford, California 94305

Director
Electronics Research Laboratory
University of California
Berkeley, California 94720

Director
Electronic Sciences Laboratory
University of Southern California
Los Angeles, California 90007

Dr. C. L. Coates, Director
Laboratories for Electronics and
Related Sciences Research
University of Texas
Austin, Texas 78712

Division of Engineering and
Applied Physics
210 Pierce Hall
Harvard University
Cambridge, Massachusetts 02138

Aerospace Corporation
P. O. Box 95085
Los Angeles, California 90045
Attn: Library Acquisitions Group

Professor Nicholas George
California Institute of Technology
Pasadena, California 91109

Aeronautics Library
Graduate Aeronautical Laboratories
California Institute of Technology
1201 E. California Blvd.
Pasadena, California 91109

Hunt Library
Carnegie Institute of Technology
Schenley Park
Pittsburgh, Pennsylvania 15213

Director, USAF Project RAND
Via: Air Force Liaison Office
The RAND Corporation
1700 Main Street
Santa Monica, California 90406
Attn: Library

The Johns Hopkins University
Applied Physics Laboratory
8621 Georgia Avenue
Silver Spring, Maryland 20910
Attn: Boris W. Kuvshinoff
Document Librarian

Dr. Leo Young
Stanford Research Institute
Menlo Park, California 94025

Mr. Henry L. Bachmann
Assistant Chief Engineer
Wheeler Laboratories
122 Cuttermill Road
Great Neck, New York 11021

School of Engineering Sciences
Arizona State University
Tempe, Arizona 85281

Engineering and Mathematical
Sciences Library
University of California at Los Angeles
405 Hilgrad Avenue
Los Angeles, California 90024

California Institute of Technology
Pasadena, California 91109
Attn: Documents Library

University of California
Santa Barbara, California 93106
Attn: Library

Carnegie Institute of Technology
Electrical Engineering Department
Pittsburgh, Pennsylvania 15213

University of Michigan
Electrical Engineering Department
Ann Arbor, Michigan 48104

New York University
College of Engineering
New York, New York 10019

Syracuse University
Dept. of Electrical Engineering
Syracuse, New York 13210

Yale University
Engineering Department
New Haven, Connecticut 06520

Airborne Instruments Laboratory
Deerpark, New York 11729

Bendix Pacific Division
11600 Sherman Way
North Hollywood, California 91605

General Electric Company
Research Laboratories
Schenectady, New York 12301

Lockheed Aircraft Corporation
P. O. Box 504
Sunnyvale, California 94088

Raytheon Company
Bedford, Massachusetts 01731
Attn: Librarian

Dr. G. J. Murphy
The Technological Institute
Northwestern University
Evanston, Illinois 60201

Dr. John C. Hancock, Director
Electronic Systems Research Laboratory
Purdue University
Lafayette, Indiana 47907

Director
Microwave Laboratory
Stanford University
Stanford, California 94305

Emil Schafer, Head
Electronics Properties Info Center
Hughes Aircraft Company
Culver City, California 90230

Department of Electrical Engineering
Texas Technological College
Lubbock, Texas 79409

Col. E. P. Gaines
Lawrence Radiation Laboratory
Livermore, California 94550